Redox Biology 69 (2024) 102996

Contents lists available at ScienceDirect

Redox Biology

journal homepage: www.elsevier.com/locate/redox

Phosphatidate phosphatase Lipin1 involves in diabetic encephalopathy pathogenesis via regulating synaptic mitochondrial dynamics

Xiaolin Han [a], Shan Huang [a], Ziyun Zhuang [a,b], Xiaochen Zhang [a,c], Min Xie [d], Nengjun Lou [a,e], Mengyu Hua [a], Xianghua Zhuang [a,e,**], Shuyan Yu [f,***], Shihong Chen [a,e,*]

[a] Depratment of Endocrinology and Metabolism, The Second Hospital of Shandong University, Jinan, 250033, China
[b] Department of Endocrinology and Metabolism, First People's Hospital of Jinan, Jinan, 250011, China
[c] Department of Clinical Medicine, Heze Medical College, Heze, 274009, China
[d] Department of Endocrinology and Metabolism, Binzhou Medical University Hospital, Binzhou, 256603, China
[e] Multidisciplinary Innovation Center for Nephrology of the Second Hospital of Shandong University, Jinan, 250033, China
[f] Department of Physiology, School of Basic Medical Sciences, Cheeloo College of Medicine, Shandong University, Jinan, 250012, China

ARTICLE INFO

Keywords:
Diabetic encephalopathy
Cognitive dysfunction
Synaptic plasticity
Synaptic mitochondrial dynamics
Lipin1
Phospholipids

ABSTRACT

Diabetic encephalopathy (DE) is a common central nervous system complication of diabetes mellitus without effective therapy currently. Recent studies have highlighted synaptic mitochondrial damages as a possible pathological basis for DE, but the underlying mechanisms remain unclear. Our previous work has revealed that phosphatidate phosphatase Lipin1, a critical enzyme involved with phospholipid synthesis, is closely related to the pathogenesis of DE. Here, we demonstrate that Lipin1 is significantly down-regulated in rat hippocampus of DE. Knock-down of Lipin1 within hippocampus of normal rats induces dysregulation of homeostasis in synaptic mitochondrial dynamics with an increase of mitochondrial fission and a decrease of fusion, then causes synaptic mitochondrial dysfunction, synaptic plasticity deficits as well as cognitive impairments, similar to that observed in response to chronic hyperglycemia exposure. In contrast, an up-regulation of Lipin1 within hippocampus in the DE model ameliorates this cascade of dysfunction. We also find that the effect of Lipin1 that regulating mitochondrial dynamics results from maintaining appropriate phospholipid components in the mitochondrial membrane. In conclusion, alterations in hippocampal Lipin1 contribute to hippocampal synaptic mitochondrial dysfunction and cognitive deficits observed in DE. Targeting Lipin1 might be a potential therapeutic strategy for the clinical treatment of DE.

1. Introduction

Diabetic encephalopathy (DE) refers to the chronic, progressive cognitive dysfunction and accompanying neurophysiological and structural changes in the brain resulting from diabetes mellitus (DM) [1]. Although the concept of DE was initially proposed early in the 1960s [2], there remain a lack of effective clinical treatments due to a vague understanding of the underlying pathophysiological mechanisms. Therefore, clarifying the pathogenesis of DE will not only be critical for comprehending the disease itself, but also for identifying therapeutic targets which can then be used for the treatment of DE.

Among the various pathogenic mechanisms of DE, synaptic plasticity impairment is strongly related to the cognitive dysfunction [3,4]. It has been suggested that mitochondrial dysfunction represents one of the main causes of synaptic plasticity impairment in resultant neurodegenerative diseases [5,6]. As mitochondria are the main sites for glucose-utilization and energy generation in the brain, synaptic mitochondrial function may be damaged due to the hyperglycemia exposure and then contribute to the damage of synaptic plasticity.

Normally, mitochondria exist in a dynamic homeostatic state, constantly adjusting their structure, shape, number and position in response to different signals from inside and outside of cells [7]. Such adaptions to the changes in environment stimuli are referred to as mitochondrial dynamics. This process consists of four distinct, but closely related pathways: mitochondrial fusion, fission, mitophagy and

* Corresponding author. The Second Hospital of Shandong University, 247 Beiyuan Street, Jinan, 250033, China.
** Corresponding author. The Second Hospital of Shandong University, 247 Beiyuan Street, Jinan, 250033, China.
*** Corresponding author. Shandong University, 44 Wenhua West Road, Jinan, 250012, China.
E-mail addresses: zhuangxianghua@email.sdu.edu.cn (X. Zhuang), shuyanyu@sdu.edu.cn (S. Yu), chenshihong@sdu.edu.cn (S. Chen).

https://doi.org/10.1016/j.redox.2023.102996
Received 28 November 2023; Accepted 11 December 2023
Available online 12 December 2023

Abbreviations

DE	diabetic encephalopathy
DM	diabetes mellitus
PAP	phosphatidate phosphatase
PA	phosphatidate
DAG	diacylglycerol
TG	triglycerides
AAV	adeno-associated virus
LV	lentivirus
TMRM	tetramethylrhodamine methyl ester
MWM	Morris water maze
BDNF	brain-derived neurotrophic factor
SYP	synaptophysin
PSD95	postsynaptic density-95
GRIN2B	glutamate receptor subunit epsilon 2B
GluR2	glutamate receptor 2
COX IV	cytochrome C oxidase IV
GAPDH	glyceraldehyde-3-phosphate dehydrogenase
HSP60	heat shock protein 60
TOMM40	translocase of outer mitochondria membrane 40
OPA1	optic atrophy 1
MFN1/2	mitofusion 1/2
DRP1	dynamin-related protein 1
FIS1	fission 1 protein
NeuN	neuron-specific nuclear protein
MAP2	microtubule-associated protein 2
PE	phosphatidylethanolamine
PC	phosphatidylcholine
PS	phosphatidylserine

transportation [7]. Homeostasis of mitochondrial dynamics plays a vital role in ultrastructural maintenance, a process which regulates almost all aspects of mitochondrial function [8]. However, the issue of whether a mitochondrial dynamics disorder is responsible for the synaptic plasticity and cognitive impairment in DE, as well as the molecular mechanisms leading to this synaptic mitochondrial dynamics disorder remain to be determined.

A critical factor required for the maintenance of mitochondrial dynamics homeostasis is the stability and integrity of mitochondrial membrane structure [9]. Therefore, an appropriate phospholipid composition on mitochondrial membrane must be maintained [10]. Our previous work has revealed that Lipin1 is involved in the cognitive impairments associated with DE [11]. Lipin1 has been shown to be involved with the activity of phosphatidate phosphatase (PAP) enzymes, which covert phosphatidate (PA) to diacylglycerol (DAG) to promote the synthesis of triglycerides (TG) and phospholipids [12]. Given this association with PAP activity, it seems likely that Lipin1 can affect the mitochondrial dynamics via regulating phospholipid synthesis. Whether this pathway may exist within synapses of the diabetic brain and can influence synaptic plasticity requires experimental verification.

Here, to determine whether Lipin1 can regulate synaptic mitochondrial dynamics via phospholipid synthesis function, and thus affect the changes in synaptic plasticity and cognitive ability associated with DE, we established DE and hippocampal Lipin1-targeted expression regulation models. Our goal with the use of these *in vivo* and *in vitro* models was to identify any new pathways that might be involved in DE pathogenesis and establish a reliable theoretical basis for the development of new targets in the treatment of DE.

2. Materials and methods

2.1. Animal care

Male Wistar rats (180–200g, 6 weeks old) were obtained from the Beijing HFK Bioscience Co. Ltd (License No.SCXK (Beijing) 2019-0008). All rats were housed under a 12 h light/dark cycle at 24 ± 2 °C in the animal laboratory of the Second Hospital of Shandong University. Prior to use in the experiments, rats were allowed to adapt to laboratory conditions for 7 days. All animal experiments were performed in accordance with the National Institutes of Health Guide for the Care and Use of Laboratory Animals (National Research Council, 1996) and were approved by the Research Ethics Committee of the Second Hospital of Shandong University (Approval No. KYLL-2022LW164).

2.2. In vivo diabetes model

After one week-adaptive feed and 12–16 h of fasting, rats were randomly divided and treated with either streptozocin (DM group) or its solvent (control group). Streptozocin (STZ, Solarbio, Beijing, China) was prepared fresh and dissolved in 0.1 M (mol/L) cold sodium citrate buffer (pH 4.5, Solarbio). Rats of the DM group received a single intraperitoneal injection (i.p.) of STZ at 55 mg/kg body weight [13], while rats of the control group were injected with equivalent volume of sodium citrate buffer. Rats with a fasting blood glucose level >300 mg/dL (16.7 mmol/L) when assessed at 7 days post-STZ injection were considered as providing a successful diabetic model [14]. Blood glucose levels and body weights were measured at 1, 2, 3, 5, 9 and 13 weeks after STZ/solvent injection.

2.3. Cell cultures and in vitro diabetes model

The PC12 (rat adrenal pheochromocytoma) cell line was purchased from the Shanghai Cell Bank of the Chinese Academy of Science (Shanghai, China). PC12 cells were cultured in 25 mM glucose Dulbecco's modifified Eagle's medium (DMEM, Gibco, California, USA), 10 % fetal bovine serum (FBS, Excell, Shanghai, China) and 1 % penicillin/streptomycin (Solarbio) at 37 °C in a humidified incubator containing 5 % CO2. The *in vitro* diabetes model was established by exchanging the normal concentration of glucose in the medium with that of a high glucose concentration medium. To generate the high glucose concentration medium, anhydrous glucose powder (Sigma-aldrich, Darmstadt, Germany) was added to the DMEM medium at the appropriate concentration. Then PH was adjusted and medium was sterilized using a 0.22 μm filter (Sevenbiotech, Beijing, China).

2.4. Virus packaging

Lipin1 overexpression and RNA-interference adeno-associated virus (AAV, AAV-Lipin1, AAV-Lipin1ShRNA) along with lentivirus (LV, LV-Lipin1, LV-Lipin1ShRNA) with their blank vectors were purchased from the Shanghai GeneChem Corporation (Shanghai, China). The titers for all AAVs and LVs listed above were 1E+12TU/mL and 2E+9TU/mL, respectively. The sequence of Lipin1ShRNA and its blank vector are available in Table S1. AAVs were used *in vivo* for hippocampal stereotaxic injection while LVs were used *in vitro* for cell transfection to regulate the expression of Lipin1.

2.5. Hippocampal stereotaxic injection

At 9 weeks post-STZ injection, rats were anesthetized with pentobarbital sodium (40 mg/kg, i.p.) and fixed onto the brain-stereotaxic apparatus (Stoelting, USA). After the skull was fully exposed, a small hole was drilled at the anchor point. AAV-Lipin1ShRNA or their blank vectors were injected into rats of control group, while AAV-Lipin1 or

their blank vectors were injected into rats of the DE group. A total of 5ul (2.5ul per side of hippocampus) AAVs was administered using a 5 μL microsyringe (Gaoge, Beijing, China) with an injection rate of 0.15 μL/min. To ensure that AAVs were transfected in sufficient hippocampal region for the subsequent synaptosomes isolation, the stereotactic coordinates were chosen at −4.2 mm A/P, ±2.8 mm L/M, −3.5 mm D/V from Bregma according to the rat brain atlas. The microsyringe was extracted 1 mm when half of the volume was injected, and then the remaining half of the volume was injected. The microsyringe remained at this site for 10min and was then gently withdrawn. The wound was carefully disinfected and sutured.

2.6. Cell transfections

PC12 cells were seeded in 96-well plates at the density of 4000 cells/well and cultured for 24 h. According to the multiplicity of infection (MOI = 100), LVs were added into the culture medium with the transfection enhancer, HitransG A (GeneChem, Shanghai, China). The culture medium was changed after 8 h. Cells were subcultured and screened with use of recommended concentrations of puromycin (MedChemExpress, New Jersey, USA) 3 days later.

2.7. Morris Water Maze (MWM)

The MWM test was conducted to evaluate the spatial learning and memory capability, as described previously [11,15]. Additional information is available in the Supplementary methods.

2.8. Synaptosomes (containing synaptic mitochondria) isolation

Hippocampal synaptosomes (containing synaptic mitochondria) were isolated using the Minute™ Synaptosome Isolation Kit (SY-052, Invent Biotechnologies, China). Rats were anesthetized with pentobarbital sodium (40 mg/kg, i.p.) and euthanized. The isolation procedure followed the operating instructions of the kit and are available in the Supplementary methods. After measuring protein concrentrations with use of the Bicinchoninic acid (BCA) method (Solarbio), synaptosomes were used for the subsequent experiments.

2.9. Cell-counting-kit 8 (CCK-8) assay

Proliferation viability of cells was determined with use of the CCK-8 assay (MedChemExpress). PC12 cells were planted into 96-well plates at the density of 3000 cells/well and cultured in complete DMEM medium. Then medium was changed to one with different glucose or mannitol concentrations and cells were cultured for 24 or 48 h. CCK-8 reagent was added to the medium at the ratio of 1:100 and incubated for 2–4 h. Proliferation viability was measured using an optical density (OD) value at the absorbance of 450 nm with a microplate reader (Biotek, Vermont, USA).

2.10. RNA extraction and real-time quantitative polymerase chain reaction (RT-qPCR)

RNA from PC12 cells or hippocampal tissues was extracted using the SteadyPure Fast RNA Extraction Kit (AG21023, Accurate Biology, Changsha, China) or Fast Tissue RNA Purification Kit (EZB-RN5, EZBioscience, USA), respectively, while cDNA synthesis was conducted with the use of *Evo M-MLV* Transcription Kit II (AG11711, Accurate Biology) according to the operating instructions. RT-qPCR was performed using the ChamQ SYBR qPCR Master Mix (Vazyme, Nanjing, China) and was detected with the use of QuantStudio™ 5 Real-time fluorescence quantitative PCR system (ThermoFisher Scientific, USA). Relative gene expression levels were calculated with the use of the classic 2 (−ΔΔCt) method. Primer sequences used are presented in Table S2.

2.11. Western blot (WB)

Tissues or cells were resuspended in the cool radio immunoprecipitation assay (RIPA) lyris buffer (Beyotime, Shanghai, China) containing 1 % protease inhibitors (MedChemExpress) and 1 % phosphatase inhibitors (MedChemExpress) for 30 min on ice. Then samples were centrifuged at 12,000 rpm for 20 min at 4 °C and the supernatant containing protein was removed. Total protein concrentration was determined with use of the BCA kit (Solarbio) and protein samples were then heated within 5 × loading buffer (Beyotime) at 99.5 °C for 10 min. Equal amounts of protein were fractionated using 8 %, 10 %, 12 % or 15 % sodium dodecyl sulfate polyacrylamide gel electrophoresis (SDS-PAGE) and then transferred onto PVDF membranes (Merck Millipore, Darmstadt, Germany). The membranes were blocked with 5 % skim milk for 1 h at room temperature and incubated overnight at 4 °C with the primary antibodies. Information regarding primary antibodies is available in Table S3. After an overnight incubation, membranes were incubated with the secondary antibodies (1:5000, Solelybio, Beijing, China) for 1 h at room temperature. Bands were detected using chemiluminescence (ECL) HRP substrate (Merck Millipore) under an chemiluminescence imager (Tanon4800, Shanghai, China).

2.12. Detection of mitochondrial membrane potentials

Acute brain slices (150 μm) of rats hippocampus were prepared using a oscillating microtome (Leica, Germany) and perfused with oxygenized artificial cerebrospinal fluid (ACSF) containing (in mM) 120 NaCl, 3.5 KCl, 2.5 CaCl2, 1.3 MgSO4, 1.25 NaH2PO4, 26 NaHCO3 and 10 glucose (Sigma, USA). Tetramethylrhodamine methyl ester (TMRM, (200 nM, MedChemExpress) was then added into oxygenized ACSF and slices were incubated for 30 min at 37 °C. After a brief wash, slices were following incubated in oxygenized ACSF containing Hoechst 33342 (10 μg/mL, Solarbio) for 5 min at 37 °C to dye the nucleus. Unfixed slices were immediately covered and observed under an confocal microscope (LSM880, Zeiss, Oberkochen, Germany).

As for analyzing the mitochondrial membrane potential of cultured cells, PC12 cells were seeded on glass bottom cell culture dishes (Sevenbiotech, China). After cultured with normal or high concentration of glucose, cells were incubated in complete medium containing 100 nM TMRM and then 10 μg/mL Hoechst 33342 for 30 min and 5 min respectively at 37 °C. Unfixed cells were immediately observed under an inverted confocal microscope (LSM800, Zeiss). Images was captured using Zeiss ZEN software.

2.13. Immunofluorescence

A description of the procedures involved with the preparation of frozen brain slices and fixed cells is contained in the Supplementary methods. After blocking, as performed using confining liquid (containing 0.2 % TritonX-100, Sevenbiotech; 5 % goat serum, Solarbio and 25 mg/ml BSA, Solarbio), frozen slices or fixed cells were incubated with primary antibody at 4 °C overnight. Information of primary antibodies used is available in Table S4. Frozen slices or cells were then incubated with Alexa Fluor 488 (ab150117, abcam, Cambridge, UK) or Alexa Fluor 594 (ab150084, abcam) for 1 h at 37 °C. Finally, DAPI (10 μg/ml, Solarbio) was used for nuclear staining. Images were captured under an inverted confocal microscope and processed by Zeiss ZEN software.

2.14. Detection of mitochondrial ROS levels

Frozen brain slices were stained with Mitosox Red fluorescent dye (5 μM, Invitrogen, California, USA) for 30 min at 37 °C and DAPI (10 μg/ml) for nuclear staining. Viable PC12 cells were stained with complete medium containing Mitosox Red fluorescent dye (5 μM) for 30 min and then Hoechst 33342 (10 μg/ml) for 5 min at 37 °C. Images were captured using an inverted confocal microscope and processed using Zeiss ZEN

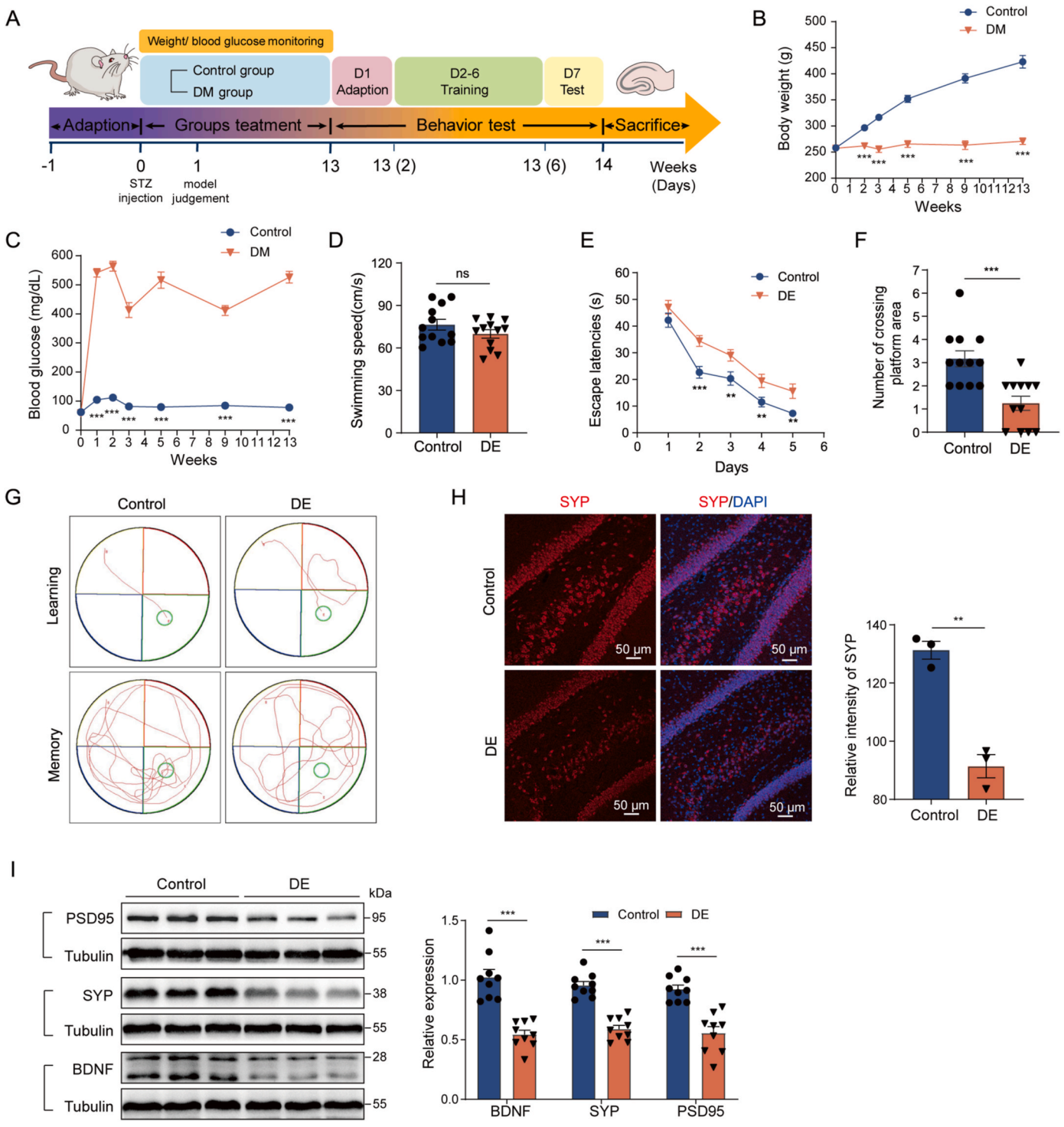

Fig. 1. Cognition and synaptic plasticity impairments in DE rats.
(A) Schematic diagram of the study design. **(B)** Body weight and **(C)** blood glucose level in control and DM rats along the course of diabetes (n = 12). **(D)** Swimming speed in control and DE rats in the Morris Water Maze (MWM) test (n = 12). **(E)** Escape latencies during the MWM training period in control and DE rats (n = 12). **(F)** Number of platform area crossing in the MWM test period in control and DE rats (n = 12). **(G)** Representative motor trajectories on the fifth day of MWM training period and the test period in control and DE rats. **(H)** Relative intensity of SYP in hippocampal sections of control and DE rats as determined using IF (n = 3). Scale bar is 50 μm. **(I)** Relative expression of BDNF, SYP and PSD95 in the hippocampus of control and DE rats as determined using WB (n = 9). All data represent means ± SEMs. $^{*}P < 0.05$, $^{**}P < 0.01$ and $^{***}P < 0.001$, by independent-samples *t*-test.

software.

2.15. Transmission electron microscopy (TEM)

The hippocampus were rapidly isolated and dissected into small tissue cubes (1 mm^3), fixed with 2 % glutaraldehyde, dehydrated with use of an ethanol gradient, embedded, and then sectioned. Samples were stained with uranyl acetate followed by lead citrate on the copper grids. The ultrastructure of hippocampal neurons, along with their synapses and mitochondria were observed under a transmission electron

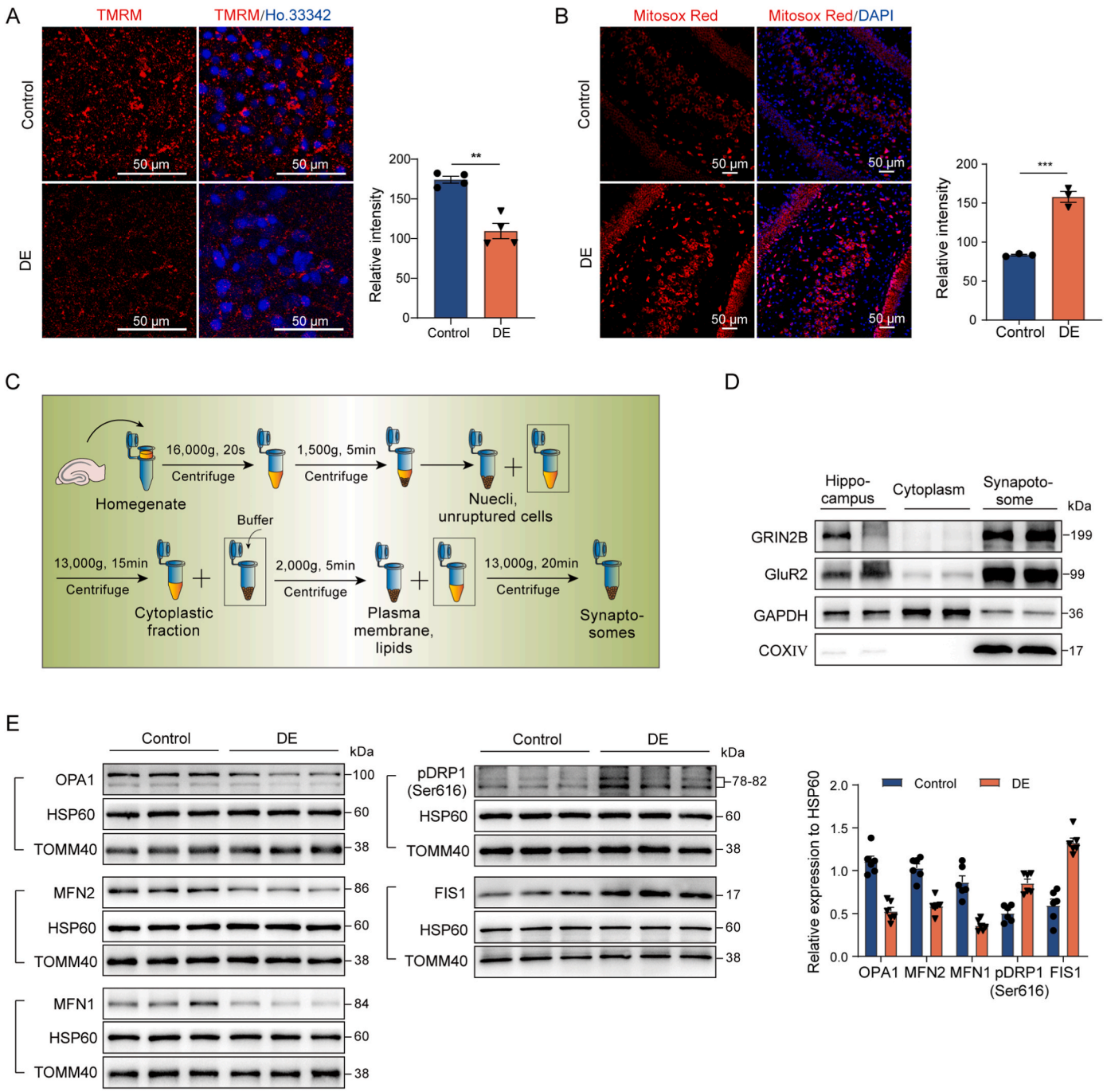

Fig. 2. Synaptic mitochondrial function and dynamics disorder in the hippocampus of DE rats.
(A) Acute brain slices obtained from hippocampus of control and DE rats were stained with TMRM to assess mitochondrial membrane potentials (n = 4). Scale bar is 50 μm. **(B)** Frozen brain slices obtained from control and DE rats were stained with Mitosox Red to evaluate the mitochondrial ROS levels (n = 3). Scale bar is 50 μm. **(C)** Schematic diagram of procedures for synaptosomal isolation by differential centrifugaion using a synaptosome isolation kit (Invent Biotechnologies, Beijing, China). **(D)** WB was used to authenticate the isolation efficiency of synaptosomes. **(E)** Expressions of the mitochondrial dynamic-related proteins, OPA1, MFN1/2, pDRP1 (Ser616) and FIS1 within synaptosomes isolated from the hippocampus of control and DE rats as evaluated using WB, and analysis of WB with HSP60 as the mitochondrial internal reference (n = 6). All data represent means ± SEMs. $^{*}P < 0.05$, $^{**}P < 0.01$ and $^{***}P < 0.001$, by independent-samples *t*-test and one-way ANOVA with LSD or Tamhane tests for post-hoc comparisons. (For interpretation of the references to color in this figure legend, the reader is referred to the Web version of this article.)

microscope (Philips Tecnai 20 U-Twin, Holland).

2.16. LC-MS/MS lipidomics

Briefly, PC12 cells were collected at 4 °C and preserved at −80 °C until lipid extraction. Lipids were extracted according to MTBE method and then analyzed using the LC-MS/MS method. Details regarding lipid extraction, analysis and identification are available in the Supplementary methods.

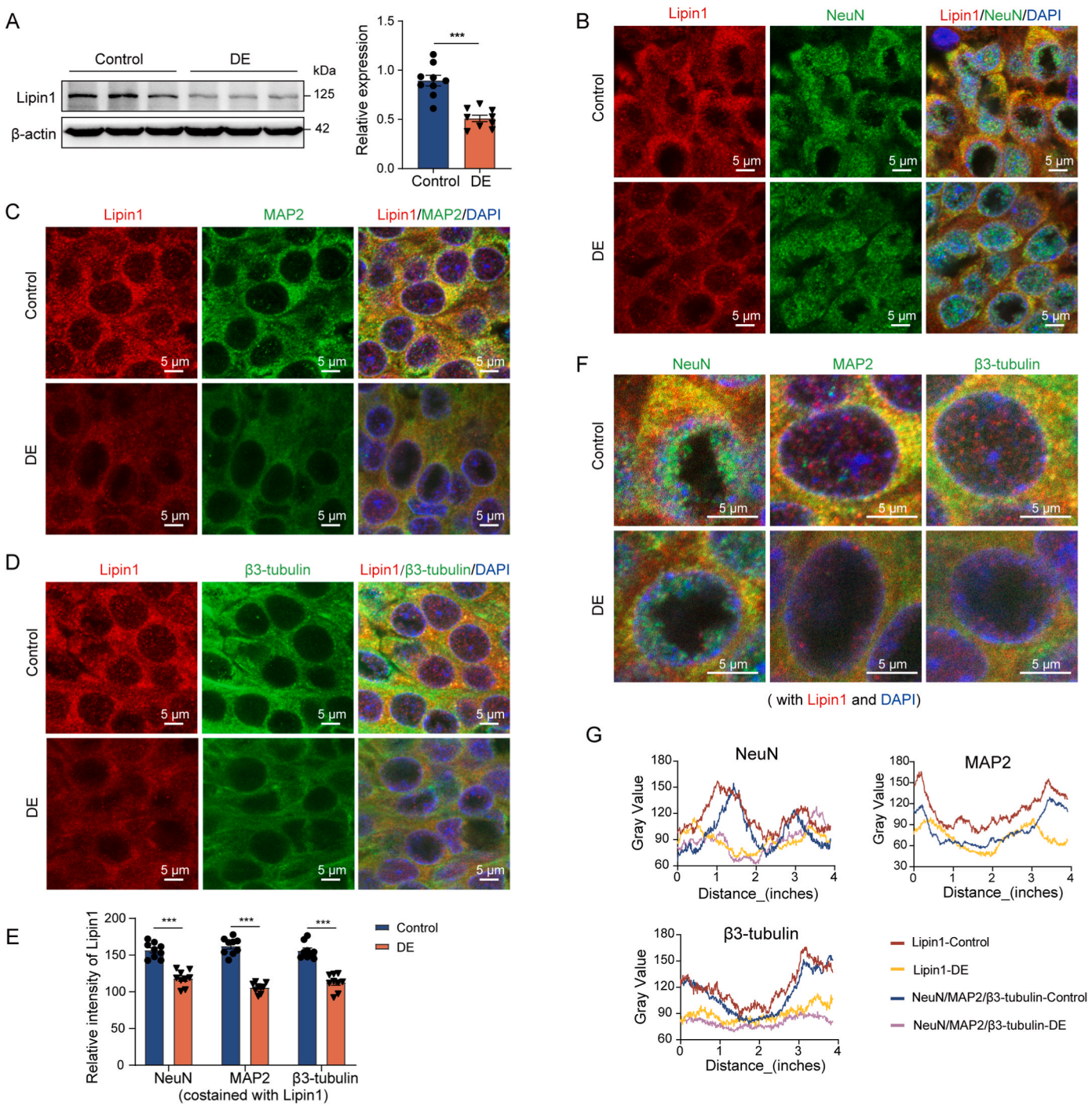

Fig. 3. Lipin1 expression within hippocampal neurons of DE rats.
(A) Expression of Lipin1 in the hippocampus of control and DE rats as determined using WB (n = 9). **(B–D)** Frozen brain slices of control and DE rats used for co-staining of Lipin1 with **(B)** NeuN, **(C)** MAP2 and **(D)** β3-tubulin. Scale bar is 5 μm. **(E)** Analysis of general relative intensities of Lipin1 between control and DE rats (n = 9 images/group). **(F)** Magnified images showing the details of co-localization. Scale bar is 5 μm. **(G)** Co-localization analysis was performed using ImageJ software. The abscissas represents the distance from the start of horizontal axis of the rectangular image and the ordinates indicate the gray value of the relevant site. All data represent means ± SEMs. $^{*}P < 0.05$, $^{**}P < 0.01$ and $^{***}P < 0.001$, by independent-samples *t*-test.

2.17. Statistical analysis

All data were expressed as means ± SEMs of independent experiments. With the exception of lipidomics, all data were analyzed with use of the IBM SPSS Statistics 22 program (SPSS Inc., Chicago, USA). Statistical significance of differences among groups was evaluated by 2 tailed independent-samples *t*-test or one-way ANOVA followed by the LSD or Tamhane tests for post-hoc comparisons. $P < 0.05$ was required for results to be considered as statistically significant.

The data of lipidomics were analyzed by R package (ropls) for multivariate data analysis, including Pareto-scaled principal component analysis (PCA) and orthogonal partial least-squares discriminant analysis (OPLS-DA). The 7-fold cross-validation and response permutation testing were used to evaluate the robustness of the model. The variable importance in the projection (VIP) value of each variable in the OPLS-DA model was calculated to indicate its contribution to the

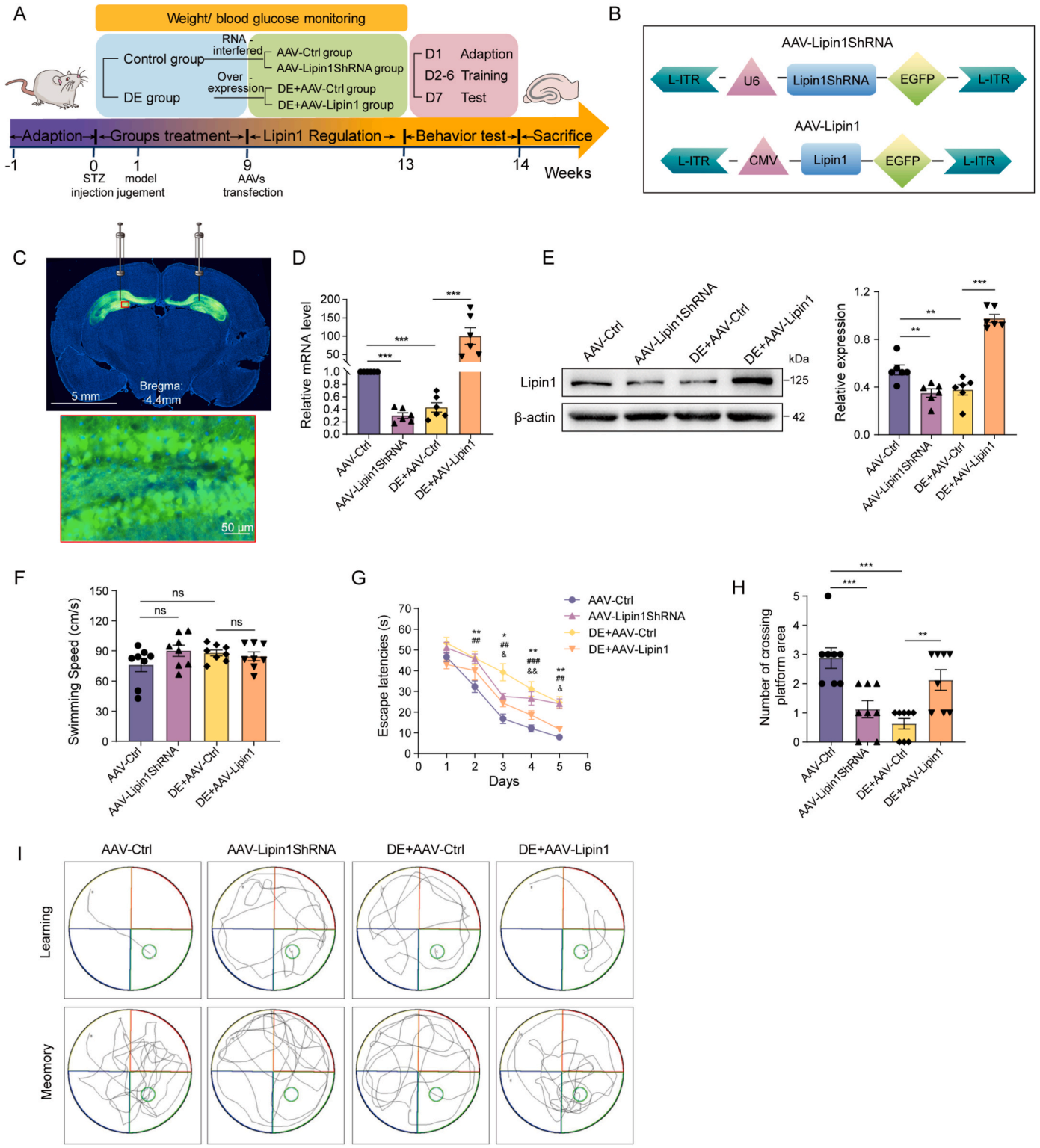

Fig. 4. Lipin1 effects upon cognitive performance.
(A) Schematic diagram of study design for Lipin1 function in hippocampus of DE rats. **(B)** Schematic diagram of element sequence of AAVs used for regulating Lipin1 expression. **(C)** Spontaneous green fluorescence within the hippocampus after AAVs injection. Scale bar is 5 mm and scale bar of magnified image is 50 μm. **(D)** Hippocampal Lipin1 mRNA levels after AAVs injection as determined using RT-qPCR (n = 6). **(E)** Hippocampal Lipin1 protein levels after AAVs injection as determined using WB (n = 6). **(F)** Swimming speeds in AAV-Ctrl, AAV-Lipin1ShRNA, DE + AAV-Ctrl and DE + AAV-Lipin1 groups in the MWM test (n = 8). **(G)** Escape latencies during the MWM training period for the four groups of rats after AAVs injection (n = 8). All data represent means ± SEMs. $^{*}P < 0.05$, $^{**}P < 0.01$, AAV-Lipin1ShRNA group versus AAV-Ctrl group; $^{\#\#}P < 0.01$, $^{\#\#\#}P < 0.001$, DE + AAV-Ctrl group versus AAV-Ctrl group; $^{\&}P < 0.05$, $^{\&\&}P < 0.01$, DE + AAV-Lipin1 versus DE + AAV-Ctrl group. **(H)** Number of platform crossings in the MWM test period for the four groups of rats after AAVs injection (n = 8). **(I)** Representative motor trajectories on the fifth day of the MWM training period and the test period as recorded from the four groups of rats after AAVs injection. All data represent means ± SEMs. $^{*}P < 0.05$, $^{**}P < 0.01$ and $^{***}P < 0.001$, by one-way ANOVA with LSD or Tamhane tests for post-hoc comparisons. (For interpretation of the references to color in this figure legend, the reader is referred to the Web version of this article.)

classification. Lipids with the VIP value > 1 was further applied to Student's t-test at univariate level to measure the significance of each lipid, $P < 0.05$ were considered as statistically significant.

3. Results

3.1. Cognitive performance and synaptic plasticity are impaired in DE rats

Male Wistar rats were randomly divided into control and DM group and diabetes model was established by one-time intraperitoneal injection of STZ (Fig. 1A). Rats within the DM group showed a dramatic decrease in body weight and an increase in blood glucose levels (Fig. 1B and C). Body fat rate within DM rats was substantially decreased as compared with that in control rats (Fig. S1A). At 12 weeks after a successful establishment of the diabetes model (13 weeks after STZ injection), Morris Water Maze (MWM) tests were conducted to evaluate the spatial learning and memory ability of these rats. No statistically significant differences in swimming speeds were obtained between rats in the control versus DE group (Fig. 1D). During the MWM training period, there was a significant increase in escape latencies (time required to locate the platform) in DE rats, which was observed starting on the second day of training (Fig. 1E, G). In the test period, DE rats demonstrated significantly fewer crossings of the platform area (Fig. 1F and G). One day after completing the MWM test, rats were euthanized and the hippocampus was removed. We found that DE rats demonstrated a significant decrease in the cognition-associated protein, including brain-derived neurotrophic factor (BDNF), as well as the synaptic function-associated protein Synaptophysin (SYP) and postsynaptic density-95 (PSD95) within these hippocampal tissue samples as determined with immunofluorescent (IF) assays (Fig. 1H) and WB (Fig. 1I). Taken together, these results demonstrate that DE rats show impairments in cognitive function and synaptic plasticity.

3.2. Synaptic mitochondrial function and homeostasis of synaptic mitochondrial dynamics are impaired in hippocampus of DE rats

As mitochondria are the main site of glucose metabolism and source of energy, we speculated that synaptic mitochondria dysfunction might contribute to the synaptic plasticity impairments in DE. We observed a significant decrease in the intensity of TMRM staining (Fig. 2A) along with an increase in Mitosox Red staining (Fig. 2B) within hippocampal sections of DE rats, indicating the presence of mitochondrial membrane potential damage and an enhancement of mitochondrial oxidative stress. To further investigate mitochondrial function within synapses, we isolated hippocampal synaptosomes, which containing synaptic mitochondria, as achieved using a synaptosome isolation kit (Invent Biotechnologies, Beijing, China). The procedure for this assay is contained within schematic diagram of Fig. 2C. Then the isolation efficiency was evaluated using WB. Compared with levels in hippocampal tissue and cytoplasmic proteins as obtained in the process of isolation, we found that synaptosomes were enriched with proteins specifically expressed in synapses (glutamate receptor subunit epsilon 2B, GRIN2B, and glutamate receptor 2, GluR2) and mitochondria (cytochrome C oxidase IV, COX IV), while they lacked proteins typically expressed within the cytoplasm (glyceraldehyde-3-phosphate dehydrogenase, GAPDH) (Fig. 2D, Fig. S1B). Such results indicated a successful isolation of synaptosomes. These isolated synaptosomes were then used for the measurement of mitochondrial complex enzyme activity. Within hippocampal synaptic mitochondria of DE rats, there was a hypoactivity of Complex I-V (Fig. S1C).

As maintenance of normal mitochondrial function requires a homeostasis of mitochondria dynamics, we next assessed the fusion and fission of synaptic mitochondria using WB. To best achieve reliable results, two types of mitochondrial internal reference proteins, heat shock protein 60 (HSP60) and translocase of outer mitochondria membrane 40 (TOMM40), were chosen as indicators of the total amount of mitochondrial protein. Interestingly, we found that the expression of fusion-associated proteins on both the inner (optic atrophy 1, OPA1) and outer (mitofusin1/2, MFN1/2) membranes of mitochondria were decreased, while expression of fission-associated proteins (phosphorylated dynamin-related protein 1, pDRP1 (ser616) and fission 1 protein, FIS1) were increased in hippocampal synaptic mitochondria of DE rats (Fig. 2E and Fig. S1D). A compilation of these results reveals that a significant disorder in synaptic mitochondrial function is present in DE rats and, this effect appears to be due to a breakdown in the homeostasis of synaptic mitochondrial dynamics.

3.3. The expression of phosphatidate phosphatase Lipin1 is decreased within the hippocampal neurons of DE rats

Previous work within our laboratory had demonstrated that phosphatidate phosphatase Lipin1 was associated with the cognitive impairment of DE. As mitochondrial membrane status is critical for the homeostasis of mitochondrial dynamics, it seemed likely that Lipin1 may play a role in regulating this process. To address this issue, we first evaluated the expression of Lipin1 and its distribution in hippocampal neurons of control and DE rats. Results of our WB showed that the expression of Lipin1 was significantly decreased within the hippocampus of DE rats (Fig. 3A). Then we used IF assay to co-stain Lipin1 with neuron-specific nuclear protein (NeuN), microtubule-associated protein 2 (MAP2) and β3-tubulin to determine Lipin1 distribution in hippocampal neurons (Fig. 3B, C, D). We found that the fluorescence intensity of Lipin1 is significantly decreased in DE hippocampus, consistent with the results of WB (Fig. 3E). We also found that Lipin1 co-stained with all three of these neuronal markers (Fig. 3F and G), so it would appear that Lipin1 is distributed widely in neuronal cytoplasm. Moreover, expression levels of Lipin1 co-stained with NeuN, MAP2 and β3-tubulin are all reduced in hippocampus of DE rats (Fig. 3G), suggesting that we can concentrate on the effect of Lipin1 deficiency upon neurons.

3.4. Lipin1 affects cognitive ability of DE rats

To further assess Lipin1 effects upon cognitive impairment in DE as well as to investigate some of the regulatory mechanisms involved, we constructed a Lipin1 RNA-interference and overexpression AAVs for the targeted regulation of Lipin1 expression. Lipin1 RNA-interference AAVs and their blank vectors were injected into the hippocampus of control rats (AAV-Lipin1ShRNA group and AAV-Ctrl group) while Lipin1 overexpression AAVs and their blank vectors were injected into the hippocampus of DE rats (DE + AAV-Lipin1 group and DE + AAV-Ctrl group) using hippocampal stereotaxic injection (Fig. 4A). The element sequences of these AAVs are presented in the schematic diagram of Fig. 4B. To identify the transfection efficiency of AAVs, panoramic scanning images of rats brain were captured, with spontaneous green fluorescence in hippocampus being observed (Fig. 4C). Results of RT-qPCR assays and WB verified that a successful regulation of Lipin1, both at transcriptional and protein expression levels, had been achieved (Fig. 4D and E). AAVs injection did not affect body weight or blood glucose level of rats (Figs. S2A and B).

At 4 weeks after injection, behavior tests were conducted. There were no significant differences in swimming speeds among the four groups within the MWM (Fig. 2F). Beginning with day two of the training period, the AAV-Lipin1ShRNA group and DE + AAV-Ctrl group showed significant increases in escape latencies as compared with that of the AAV-Ctrl group, whereas the DE + AAV-Lipin1 group showed decreased escape latencies versus that of the DE + AAV-Ctrl group beginning on the third day of training (Fig. 4G, I). During the MWM test period, rats of the AAV-Lipin1ShRNA and DE + AAV-Ctrl groups crossed the platform area significantly less often than the AAV-Ctrl group, whereas the DE + AAV-Lipin1 group crossed this platform significantly more often than that of the DE + AAV-Ctrl group (Fig. 4H and I). These MWM results imply that a reduction of Lipin1 expression impairs the

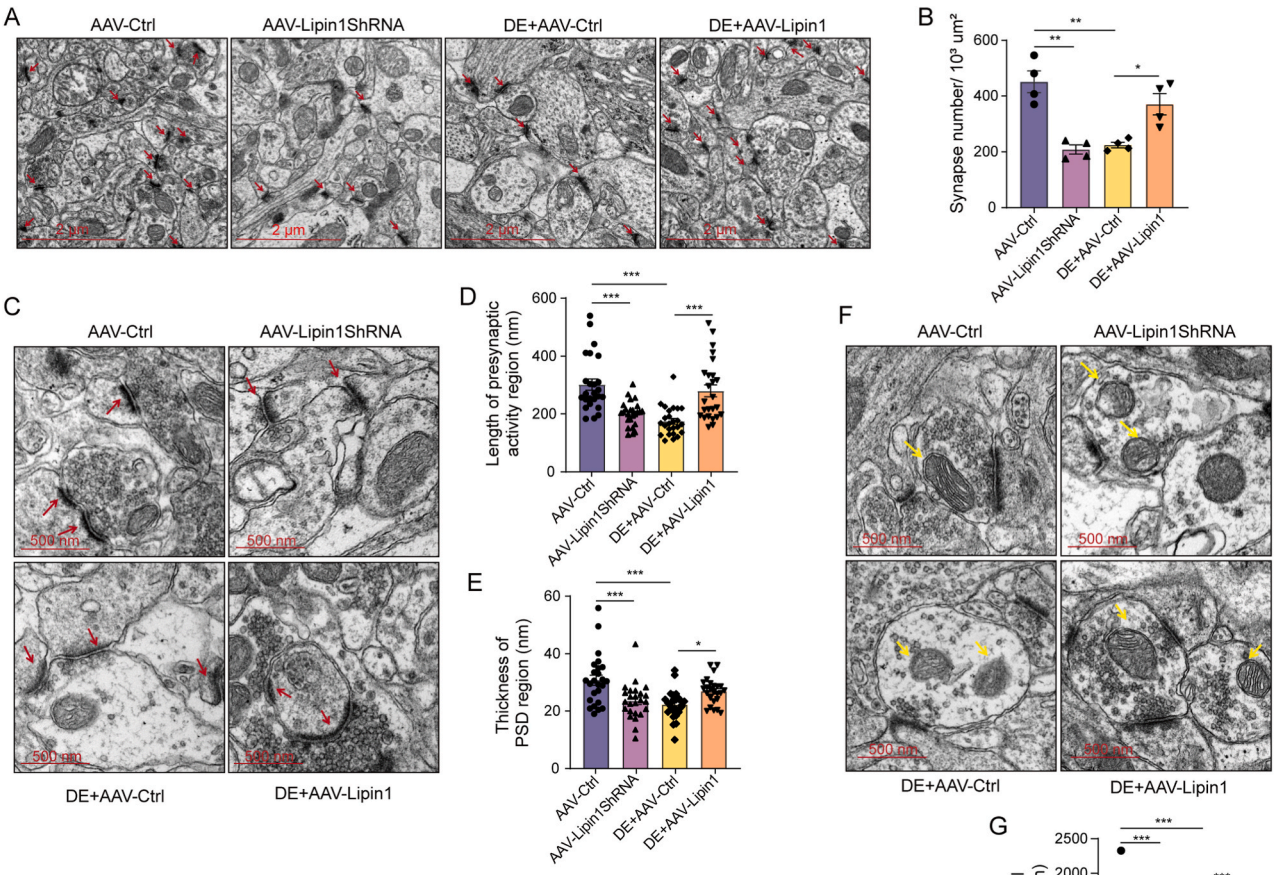

(caption on next page)

Fig. 5. Lipin1 effects upon hippocampal synaptic plasticity, synaptic mitochondrial function and dynamics.
(A) Representative TEM images of synapses. Red arrows indicate location of synapses. The scale bar is 2 μm. **(B)** Analysis of synaptic densities in the hippocampus after AAVs injection, as indicated by the number of synapses within a 10^3 μm^2 section area (n = 4). **(C)** Representative images of synaptic ultrastructure under high power field magnification. Red arrows indicate the location of synapses. Scale bar is 500 nm. **(D)** Analysis of length of the presynaptic membrane active region within the hippocampus after AAVs injection (n = 25 synapses/group). **(E)** Analysis of thickness of the PSD region within the hippocampus after AAVs injection (n = 25 synapses/group). **(F)** Representative images of synaptic mitochondrial ultrastructure within the hippocampus after AAVs injection. Yellow arrows indicate synaptic mitochondria. Scale bar is 500 nm. **(G)** Analysis of perimeter of single synaptic mitochondrion within the hippocampus after AAVs injection (n = 15 synaptic mitochondria/group). **(H)** Mitosox Red staining was used to evaluate hippocampal mitochondrial ROS levels in the four groups after AAVs injection (n = 4). Scale bar is 50 μm. **(I)** Relative expressions of proteins related to mitochondrial dynamics from isolated hippocampal synaptosomes after AAVs injection as determined using WB and analysis with HSP60 used as the mitochondrial internal reference (n = 6). All data represent means ± SEMs. $^*P < 0.05$, $^{**}P < 0.01$ and $^{***}P < 0.001$, by one-way ANOVA with LSD or Tamhane tests for post-hoc comparisons. (For interpretation of the references to color in this figure legend, the reader is referred to the Web version of this article.)

spatial learning and memory ability of rats, while a supplement of Lipin1 to diabetic hippocampus leads to an improvement in their cognitive performance.

3.5. Lipin1 affects synaptic plasticity in the hippocampus of DE rats

After completing MWM, rats were euthanized, the hippocampus were removed and frozen slices were prepared. TEM was used to observe the ultrastructure of the neurons and synapses within these groups. Synapse number densities within the AAV-Lipin1ShRNA and DE + AAV-Ctrl groups were significantly decreased as compared with that in the AAV-Ctrl group, while significantly increased in the DE + AAV-Lipin1 group versus DE + AAV-Ctrl group (Fig. 5A and B). With regard to synapse ultrastructure, we observed a decrease in lengths of the presynaptic membrane active region (Fig. 5C and D) and thickness of the PSD region (Fig. 5C, E) in the AAV-Lipin1ShRNA and DE + AAV-Ctrl groups as compared with the AAV-Ctrl group, while increases were observed in the DE + AAV-Lipin1 group versus DE + AAV-Ctrl group. BDNF, as well as SYP and PSD95 expression were reduced in hippocampal tissue samples within the AAV-Lipin1ShRNA and DE + AAV-Ctrl groups as compared with that observed in the AAV-Ctrl group, whereas these expressions were increased in the DE + AAV-Lipin1 versus DE + AAV-Ctrl group (Figs. S2C and D). From these findings we inferred that Lipin1 can regulate synaptic plasticity within the hippocampus, and whereas an inhibition of Lipin1 expression contributes to synaptic impairment as observed in DE rats.

3.6. Lipin1 regulates synaptic mitochondrial dynamics and mitochondrial oxidative stress levels in the hippocampus of DE rats

When viewing mitochondrial ultrastructure within synapses using TEM, we found that the majority of synaptic mitochondria appeared elliptical with clear and integrated outline and cristae, and the perimeter of single mitochondrion is longer in AAV-Ctrl and DE + AAV-Lipin1 groups. Whereas in AAV-Lipin1ShRNA and DE + AAV-Ctrl groups, a greater degree of swelling in synaptic mitochondria along with vague cristae and increased amounts of mitochondrial vacuolation were observed, and the single mitochondrion appeared smaller and more rounded with a shorter perimeter (Fig. 5F and G). Results from Mitosox Red staining indicated that mitochondrial ROS levels were increased following the knock-down of Lipin1 expression, while supplementing Lipin1 within the hippocampus of DE rats reduced mitochondrial oxidative stress (Fig. 5H). After isolating hippocampal synaptosomes, we then assessed the proteins associated with mitochondrial dynamics using WB. The mitochondrial fusion-associated proteins, OPA1, MFN1/2, were significantly decreased, while the fission-associated proteins, p-DRP1 (Ser616) and FIS1 significantly increased in the AAV-Lipin1ShRNA and DE + AAV-Ctrl groups versus the AAV-Ctrl group. There was a recovery of fusion-associated proteins and a significant decline in fission-associated proteins in the DE + AAV-Lipin1 group versus the DE + AAV-Ctrl group (Fig. 5I and Fig. S2E), results which were consistent with that obtained from TEM.

Taken together, these results suggest that the decrease in hippocampal Lipin1 expression associated with DE induces an imbalance within the homeostasis of synaptic mitochondrial dynamics, an effect attribute to an up-regulation of fission and down-regulation of fusion. This disruption leads to mitochondrial fragmentation in morphology and further damages mitochondrial function, synaptic plasticity and eventually cognitive ability.

3.7. The expression of Lipin1 is decreased in PC12 cells cultured in high glucose

We next used the PC12 (rat adrenal pheochromocytoma) cell line as an *in vitro* model of neurons to investigate the mechanisms of Lipin1 regulation upon mitochondrial dynamics. The general design of this experiment is illustrated in the schematic diagram of Fig. 6A. PC12 cells were initially cultured in different concentrations of glucose (25, 50, 75, 100, 125, 150 mmol/L, mM) for either 24 or 48 h with cell viability then assessed using the CCK-8 assay. To exclude the influence of osmotic pressure, the same concentration of mannitol was simultaneously established. PC12 cell viability was decreased along with the increase of glucose concentration and culture time and we chose the 100 mM at 48h as the conditions for establishing the *in vitro* diabetes model (high glucose group, HG) (Fig. 6B, Fig. S3A). We found that Lipin1 was significantly decreased in 100mM/48h glucose group as compared with 25 mM conditions, while no significant differences were observed in 100mM/48h mannitol group (Fig. 7C). Results from the IF assay also indicated a decreased level of Lipin1 expression in the HG group versus control group (Fig. S3B).

3.8. Lipin1 regulates phospholipid components in PC12 cells

We then constructed Lipin1 RNA-interference lentiviruses (LVs) as well as their blank vectors and Lipin1 overexpression LVs as well as their blank vectors and transfected these LVs into PC12 cells (Fig. 6A). A successful transfection of LVs was observation of spontaneous green fluorescence (Fig. 6D). The element sequences of LVs are presented in the schematic diagram of Fig. 6E. Lipin1 mRNA level showed a successful regulation of Lipin1 in these cells (Fig. 6F). Then cells transfected with Lipin1 RNA-interference LVs and their blank vectors were cultured in 25 mM glucose (LV-Lipin1ShRNA and LV-Ctrl groups), while cells transfected with Lipin1 overexpression LVs and their blank vectors were cultured in 100 mM glucose for 48 h (HG + LV-Lipin1 and HG + LV-Ctrl groups). Results from the WB assay indicated that Lipin1 protein expression level was also successfully regulated by LVs transfection (Fig. 6G). Cell viability was determined with use of the CCK-8 assay. We found that cell viability within the LV-Lipin1ShRNA and HG + LV-Ctrl groups was significantly decreased compared with that of the LV-Ctrl group, while cells within the HG + LV-Lipin1 group showed an increased degree of viability versus that observed in the HG + LV-Ctrl group (Fig. S4A). These results indicate that a sufficient amount of Lipin1 can serve to maintain a normal growth profile of PC12 cells.

Then we assayed lipidomics using LC-MS/MS within the cells from the four groups receiving transfections. We authenticated a total of 35 classes and 2805 species of lipids according to the classification criteria

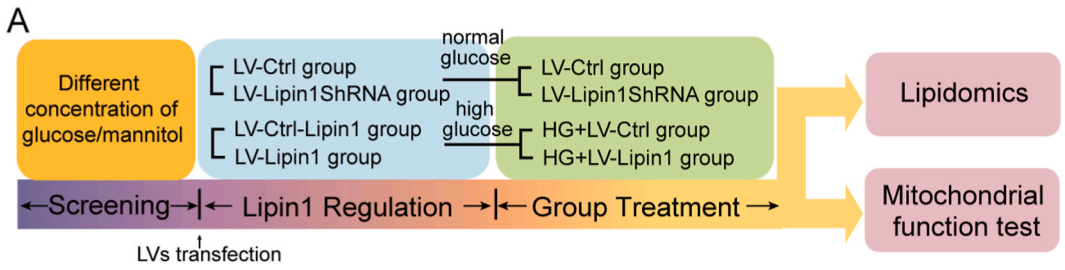

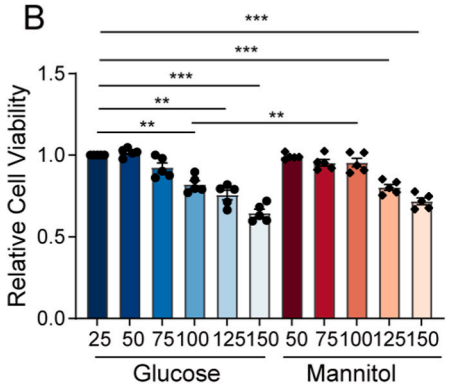

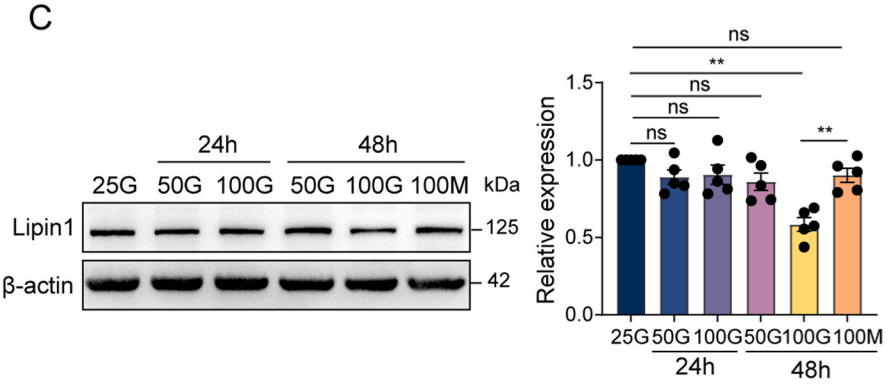

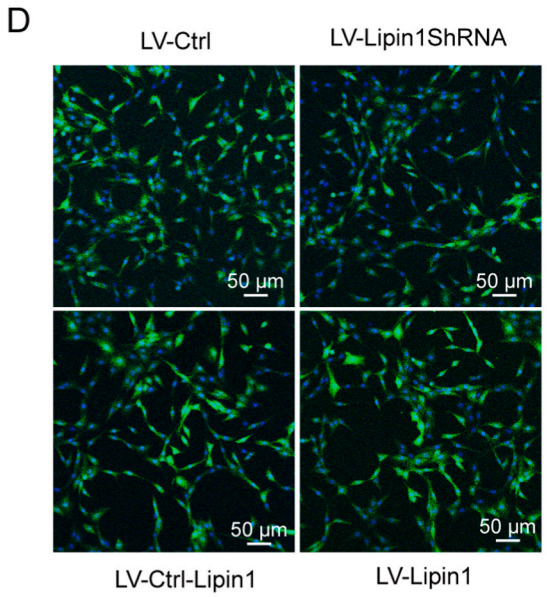

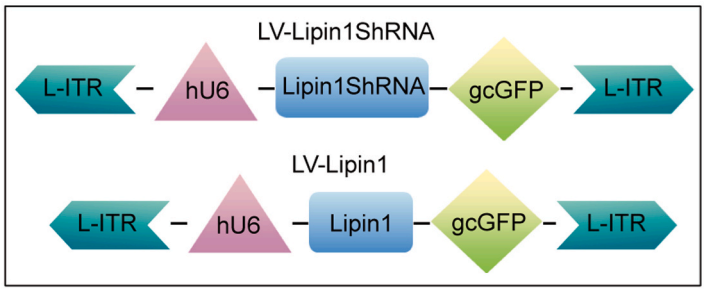

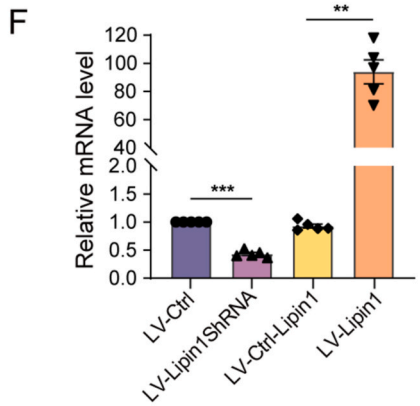

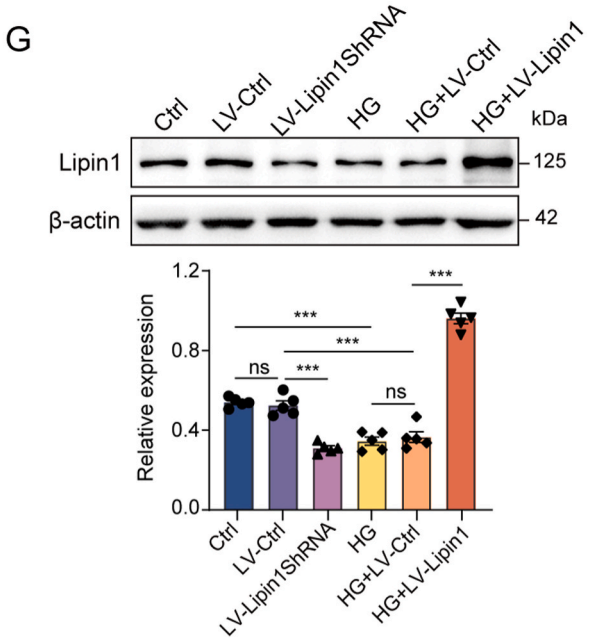

(caption on next page)

Fig. 6. Lipin1 expression levels in an *in vitro* diabetes neuronal model and the Lipin1-targeted regulation *in vitro*.
(A) Schematic diagram of the study design *in vitro*. **(B)** Changes in cell viability when PC12 cells were cultured in different concentrations of glucose and mannitol for 48 h as determined with a CCK-8 assay (n = 5). **(C)** Expression levels of Lipin1 within PC12 cells cultured in 25 mM glucose, in 50 or 100 mM glucose for 24/48 h and in 100 mM mannitol for 48 h as determined using WB (n = 5). **(D)** Spontaneous green fluorescence of PC12 cells after LVs transfection. Scale bar is 50 μm. **(E)** Element sequences of LVs used for regulating Lipin1 expression. **(F)** Relative mRNA levels of Lipin1 in PC12 cells after LVs transfection as determined using RT-qPCR (n = 5). **(G)** Expression levels of Lipin1 in PC12 cells within the control, LV-Ctrl, LV-Lipin1ShRNA, HG, HG + LV-Ctrl and HG + LV-Lipin1 groups as determined using WB (n = 5). All data represent means ± SEMs. $^{*}P < 0.05$, $^{**}P < 0.01$ and $^{***}P < 0.001$, by independent-samples *t*-test and one-way ANOVA with LSD or Tamhane tests used for post-hoc comparisons. (For interpretation of the references to color in this figure legend, the reader is referred to the Web version of this article.)

of the International Lipid Classification and Nomenclature Committee (Fig. S4B). The total amount of lipid content was significantly decreased in the LV-Lipin1ShRNA and HG + LV-Ctrl groups as compared with that of the LV-Ctrl group, while the overexpression of Lipin1 in PC12 cells exposed to high glucose significantly increased lipid content (Fig. 7A). A Venn diagram was used to present the number and overlap of lipid molecules with significant differences obtained between the LV-Ctrl and LV-Lipin1ShRNA groups, LV-Ctrl and HG + LV-Ctrl groups, HG + LV-Ctrl and HG + LV-Lipin1 groups (Fig. 7B). Bubble diagrams were used to present the class and significance of differential lipid molecules. A large number of classes of phospholipid molecules were found to be significantly different between the three pairs of contrast groups (Fig. 7C). Based on the known function of Lipin1, we focused on phosphatidylethanolamine (PE), phosphatidylcholine (PC), phosphatidylserine (PS, could be partly synthesized from PE and PC [16]) and DAG, with a hierarchical clustering analysis then being performed to evaluate the different expression patterns among the four groups. Molecules which were significantly differential within all three pairs of contrast groups were selected for presentation. From the analysis diagram, we obeserved a general tendency for a decrease in most of the PE, PC, PS and DAG molecules in the LV-Lipin1ShRNA and HG + LV-Ctrl groups as compared with that of the LV-Ctrl group, while there was a general tendency for an increase in these lipid molecules in the HG + LV-Lipin1 group versus the HG + LV-Ctrl group (Fig. 7D). Therefore, we next analyzed the amount of lipids according to lipid subclass among these four groups. We found that PC, PE, PS and DAG were significantly down-regulated when cells were cultured in high glucose or with Lipin1 knock-down. In contrast, these classes of lipids were up-regulated when Lipin1 was supplemented to these cells exposed to high glucose. In addition, PS levels were significantly decreased in the HG + LV-Ctrl group versus both the LV-Ctrl and HG + LV-Lipin1 groups, while a tendency for a decrease was observed between the LV-Lipin1ShRNA and LV-Ctrl groups, but this difference failed to achieve significance (Fig. 7E).

3.9. Lipin1 regulates mitochondrial dynamics and maintain mitochondrial function in PC12 cells

As phospholipid components, the main content of mitochondrial membranes, were significantly altered by changes in Lipin1 expression, we then investigated the effect of Lipin1 on mitochondrial morphology and function among these four groups. More mitochondrial fragmentation was observed in LV-Lipin1ShRNA and HG + LV-Ctrl groups with the use of MitoTracker staining (Fig. S4C). Results from TMRM (Fig. 8A) and Mitosox Red (Fig. 8B) staining indicated that mitochondrial membrane potential were damaged and mitochondrial oxidative stress were enhanced in the LV-Lipin1ShRNA and HG + LV-Ctrl groups versus the LV-Ctrl group, whereas a recovery in these parameters was observed in the HG + LV-Lipin1 versus HG + LV-Ctrl group. WB assays were then used to evaluate mitochondrial dynamics, with both HSP60 and β-actin serving as internal reference. In response to an interference in Lipin1 expression, MFN2 was down-regulated and pDRP1 (Ser616) was up-regulated, while MFN2 increased and pDRP1 (Ser616) decreased following Lipin1 supplement to cells cultured in high glucose (Fig. 8C and Fig. S4C). These findings suggest that Lipin1 has the capacity to regulate the balance of mitochondrial fusion and fission in neurons.

When collating all the results as presented above, it appears that Lipin1 is critical for the homeostasis maintenance of synaptic mitochondrial dynamics, an effect achieved through regulating the synthesis and composition of phospholipids within the mitochondrial membrane. With reduction in Lipin1, as can be induced by high blood glucose levels, synaptic mitochondrial function and synaptic plasticity are impaired, and eventually leading to the cognitive dysfunction observed in DE. While increasing the expression of Lipin1 in hippocampus of DE rats significantly ameliorates the synaptic plasticity impairment and cognitive dysfunction.

4. Discussion

There is increasing evidence of late that central nervous system damage induced by hyperglycotoxicity in DM shows similar pathological features with that of Alzheimer's disease (AD), from which the concept of diabetic encephalopathy (DE) is proposed [1]. It has been speculated that AD and DE share a common pathogenesis based on the higher morbidity rates of cognitive impairment in DM patients as revealed from various epidemiological researches [17]. Although findings from a number of studies have suggested some of the bases for DE pathogenesis, overall it remains a mystery due to the complex and interconnective pathways involving various gradations of molecules, neurocytes and encephalic regions [1,18,19]. In this study, we found that the decrease in phosphatidate phosphatase Lipin1 in response to hyperglycemia can alter hippocampal synaptic mitochondrial dynamics through affecting phospholipid components of mitochondrial membranes. As a result, this can lead to synaptic mitochondrial dysfunction, synaptic plasticity impairment and finally the cognitive dysfunction observed in DE.

In this report, we found that rats in the DE group showed a decline in their ability for spatial learning and memory, effects which resemble that observed in animal models of AD. Such results are consistent with our previous study [11] as well as that reported by others using different models of diabetes [3,20,21]. Among the mechanisms believed to be involved with DE, we concentrated on the hippocampal synaptic plasticity, as it represents an essential process required for the effective transmission of nerve impulses in the learning and memory [22]. We found that decreases in BDNF, SYP and PSD95 expressions were present in DE rats, results which are in agreement with previous studies on synaptic plasticity and DE [15,23]. Interestingly, the changes in synaptic plasticity resulting from DE share similar features to that observed in AD [24,25], which provides an explanation for the similarities in cognitive dysfunction as manifested in both DE and AD.

Almost every physiological activity associated with synapses requires energy, which is provided by mitochondria [5]. In this study, we evaluated different aspects of mitochondrial function in DE models. We assessed mitochondrial membrane potentials, which are generated by oxidative phosphorylation (OXPHOS) [26] and are essential for other mitochondrial functions [27,28]. We found that a reduction in mitochondrial membrane potential was present in the DE group, an effect which also occurs in AD [29]. Mitochondria are the main source of ROS, generated through the electron transport chain (ETC) as performed by mitochondrial complex I-IV [30]. Excessive ROS can result in irreversible mitochondrial impairments leading to insufficient ATP generation, as well as oxidative cell damage and pro-inflammatory reactions [31]. Enhanced hippocampal mitochondrial ROS was observed in the DE group of our study. Such results indicate excessive oxidative stress as a common pathological change in hyperglycemic brain injury, as reported

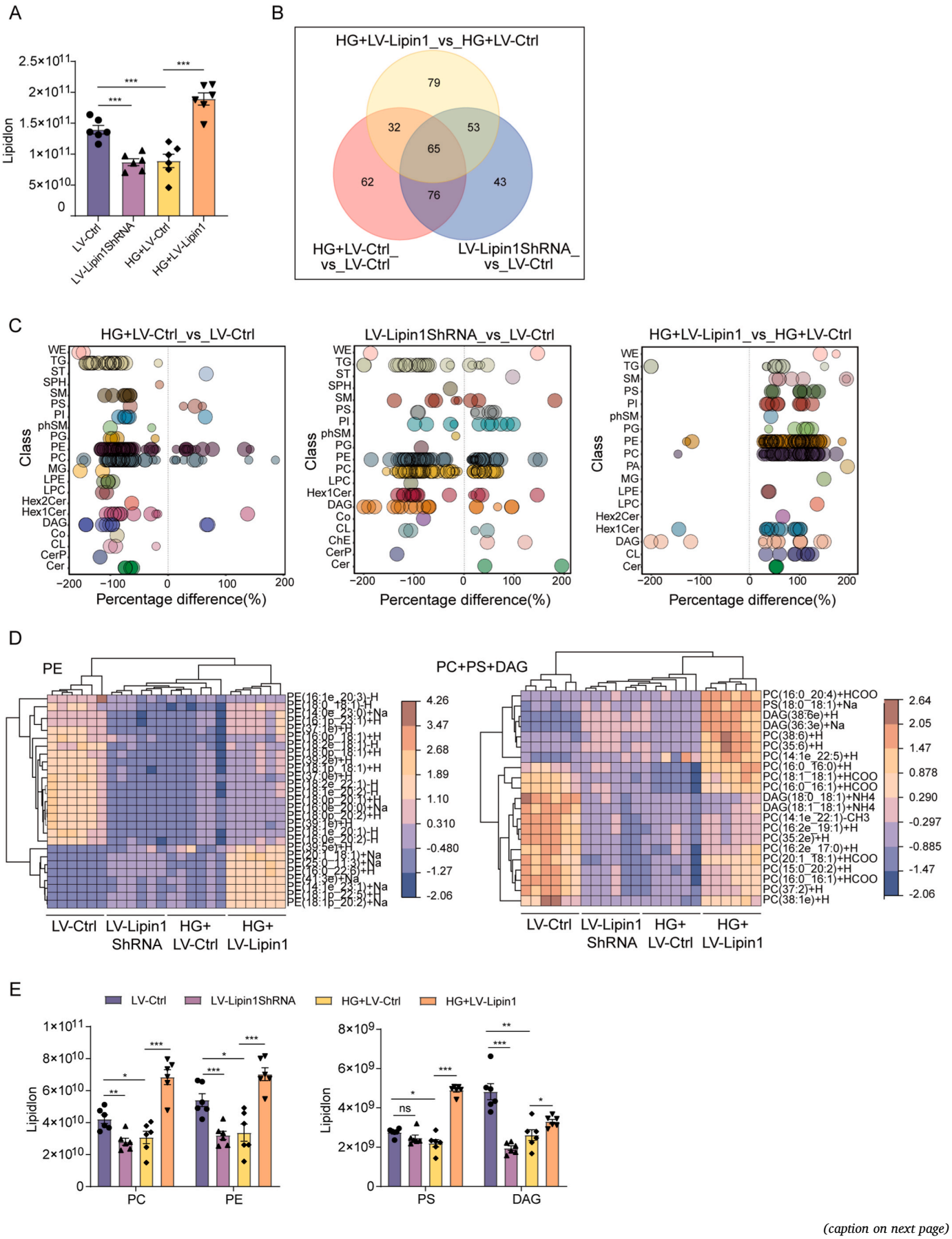

(caption on next page)

Fig. 7. Lipin1 effects upon phopsholipid components in PC12 cells.
(A) Total lipid quantity of PC12 cells in LV-Ctrl, LV-Lipin1ShRNA, HG + LV-Ctrl and HG + LV-Lipin1 groups (n = 6). **(B)** Venn diagram illustrating the overlap of significant differential lipid molecules in each pair of contrast groups (LV-Lipin1ShRNA vs LV-Ctrl; HG + LV-Ctrl vs LV-Ctrl; HG + LV-Lipin1 vs HG + LV-Ctrl). **(C)** Bubble diagrams illustrating the presence of the differential lipid molecules and their significance of differences between each pair of contrast groups (n = 6). Vertical coordinates represent each lipid subclass, which is distinguished by different colors; Bubble size represents the significance of differences, with smaller bubbles representing significant differences ($0.01 < P < 0.05$) while larger bubbles are representing extremely significant differences ($P < 0.01$). **(D)** Hierarchical clustering heat maps showing the expression patterns of PE, PC, PS and DAG (n = 6). Molecules selected to present are those significantly differential in each pair of contrast groups. **(E)** Quantity of the subclass lipids, PC, PE, PS, and DAG in the four groups after LVs transfection (n = 6). All data represent means ± SEMs. $^{*}P < 0.05$, $^{**}P < 0.01$ and $^{***}P < 0.001$, by univariate statistical analysis (Fold change analysis, independent-samples *t*-test) combined with multivariate statistical analysis (principle component analysis, PCA; partial least squares discrimination analysis, PLS-DA; orthogonal partial least squares analysis, OPLS-DA). VIP>1 and $P < 0.05$ as analyzed by OPLS-DA are considered as the screening criteria for discriminating among statistically significant differential lipids. (For interpretation of the references to color in this figure legend, the reader is referred to the Web version of this article.)

in various previous studies utilizing DE models [32,33]. Excessive ROS production also implies an increase in proton leakage due to an impairment in mitochondrial complex enzyme activity. We tested the enzyme activity of complex I–V after isolating synaptosomes from hippocampal tissue and found that all were significantly decreased in the DE group, indicating an energy metabolic defect and ATP-generating disorder in these synaptic mitochondria. Similarly, mitochondria isolated from autopsied AD brains manifest a generalized reduction in all ETC complexes, as well as some additional specific defects [34].

Mitochondrial dynamics including the balance of fusion and fission is vital for appropriate homeostasis in mitochondrial function [35]. Within AD brains there are variations in neuronal mitochondrial number and size suggesting that there is an increase of fragmented mitochondria [36]. For effective fusion and fission there needs to be participation involving a group of large GTPase domain-containing proteins such as OPA1, MFN1 and MFN2 for fusion, and DRP1 and FIS1 for fission [37]. In particular, post-translational modifications of DRP1 can produce a dual regulatory effect upon mitochondrial fission, with the promotion of fission by Ser616 phosphorylation and inhibition of fission by Ser637 phosphorylation [38]. In AD brains, significant reduction in the expressions of OPA1, MFN1 and MFN2 along with increasing levels of FIS1 are present [36,39]. While it remains controversial as to whether expression levels of DRP1 increase in AD, there is some evidence for changes in post-translational modifications of DRP1, as indicated by the significant increase in phosphorylation at Ser616 sites [36]. In contrast to that of AD, few studies regarding changes in mitochondrial dynamics exist for DE. Chen Z et al. reported that the expression of DRP1 mRNA and activity of DRP1 protein were abnormally elevated in the hippocampus of STZ-induced type 1 diabetic rats [40]. Here, we determined the expressions of mitochondrial dynamics-related proteins in isolated hippocampal synapotosomes and found that OPA1 and MFN1/2 were down-regulated, while phosphoDRP1 (ser616) and FIS1 were up-regulated in the DE group. These findings suggest that there was a fragmentation in synaptic mitochondria within the hippocampus of DE. Such fragmented mitochondria can result in an improper complex assembly critical for ETC function and the enhance ROS generation [41,42], effects which are consistent with the results as described above and can provide an explanation for the synaptic mitochondrial bioenergetics deficits in the hippocampus of DE rats.

It is well established that the inner and outer membranes of mitochondria are composed of phospholipid components which constitute the basic skeletal structure of the membrane, with protein components being embedded on it [43]. There is some evidence indicating that phospholipids can interact with dynamin GTPases by directly affecting the biological properties of mitochondrial membranes [16]. In addition to hyperglycemia, there is a general consensus that altered lipid metabolism is another characteristic of DM and is responsible for several of the other diabetes-related complications, including diabetic neuropathy [44]. We have demonstrated previously that the knockout of a type of phosphatidate phosphatase Lipin1 induced cognitive impairments resembling AD in mice [45]. And, another one of our findings that Lipin1 was significantly decreased within the hippocampus suggested that this decrease might lead to the cognitive impairments observed in DE [11]. To determine which kind of neural cells contributes most to this decrease of Lipin1, we used immunofluorescent co-staining and detected that the expression of Lipin1, which distributes widely in neuronal cytoplasmic, was diffusely reduced in whole neurons in the hippocampus of DE rats. Therefore it provides the possibility for Lipin1 to involve in the regulation of synaptic function.

In an attempt to clarify the function of Lipin1 in the pathogenesis of DE, we employed AAVs vectors as means to regulate Lipin1 expression and transfected these into hippocampus. We first verified that Lipin1 was critical in maintaining cognitive ability and synaptic plasticity in DE, consistent with that observed in our previous study [11]. Following, with a deficiency of Lipin1 there was enhanced ROS production and promotion of synaptic mitochondrial fragmentation, while the functional disorder and fusion/fission imbalance resulting from hyperglycotoxicity were partly corrected with the addition of Lipin1 into the hippocampus of DE rats.

To detect any potential change in lipid molecular quantity and composition after regulating Lipin1 expression in our *in vitro* model, we assessed lipidomics as based on a LC-MS/MS assay. Phospholipid synthesis requires participation of a diacylglycerol unit that is acquired by DAG itself or from CDP-diacylglycerol (CDP-DAG), both of which are generated from phosphatidic acid (PA). Notably, Lipin1 is the key enzyme with PAP activity for PA translation to DAG [46], which then enables this DAG to contribute to the synthesis of PE and PC via the Kennedy pathway [47]. Our current results reveal that DAG, as well as PE, PC and PS, were all decreased in PC12 cells that were treated with either high glucose or Lipin1 knock down, while the supplement of Lipin1 into PC12 cells cultured in high glucose increased these quantities of lipids above. These findings demonstrate a clear link between changes in phospholipid imbalance and Lipin1 deficiency in response to hyperglycemia. PE and PC comprise the vast majority of phospholipids (>70 %) within mitochondrial membranes [46,48] and they are essential to maintain the integrity of membrane and mitochondrial fusion and fission balance [43]. The significance of PE is particularly notable. PE has conical shape due to a small head group diameter relative to its acyl chains, a structure that produces membrane curvatures and therefore is beneficial for the fusion of mitochondria [16]. It has been reported that the lack of PE obstructs lateral movements of lipids in mitochondrial membranes with a slow mixture of lipids being observed after fusion [49]. Moreover, PE is important for the biogenesis of OPA1/Mgm1, which is directly associated with mitochondrial fusion [16]. Although the importance of phospholipids in the process of mitochondrial fission had been demonstrated in prevous studies, many of these studies employed liposomes with mixed phospholipids, which results in unclear phospholipid specificity [16,50]. Imbalance of mitochondrial fusion and fission caused by the change of phospholipid composition further leads to mitochondrial dysfunction, and it is corroborated from results as obtained with the determinations of mitochondrial membrane potential, ROS levels, mitochondrial morphology and expression of dynamics protein in PC12 cells after regulating Lipin1 expression.

Although few investigations exist regarding Lipin1 function in neurodegenerative diseases, there has been some work which has focused on the influence of Lipin1 upon mitochondrial morphology or

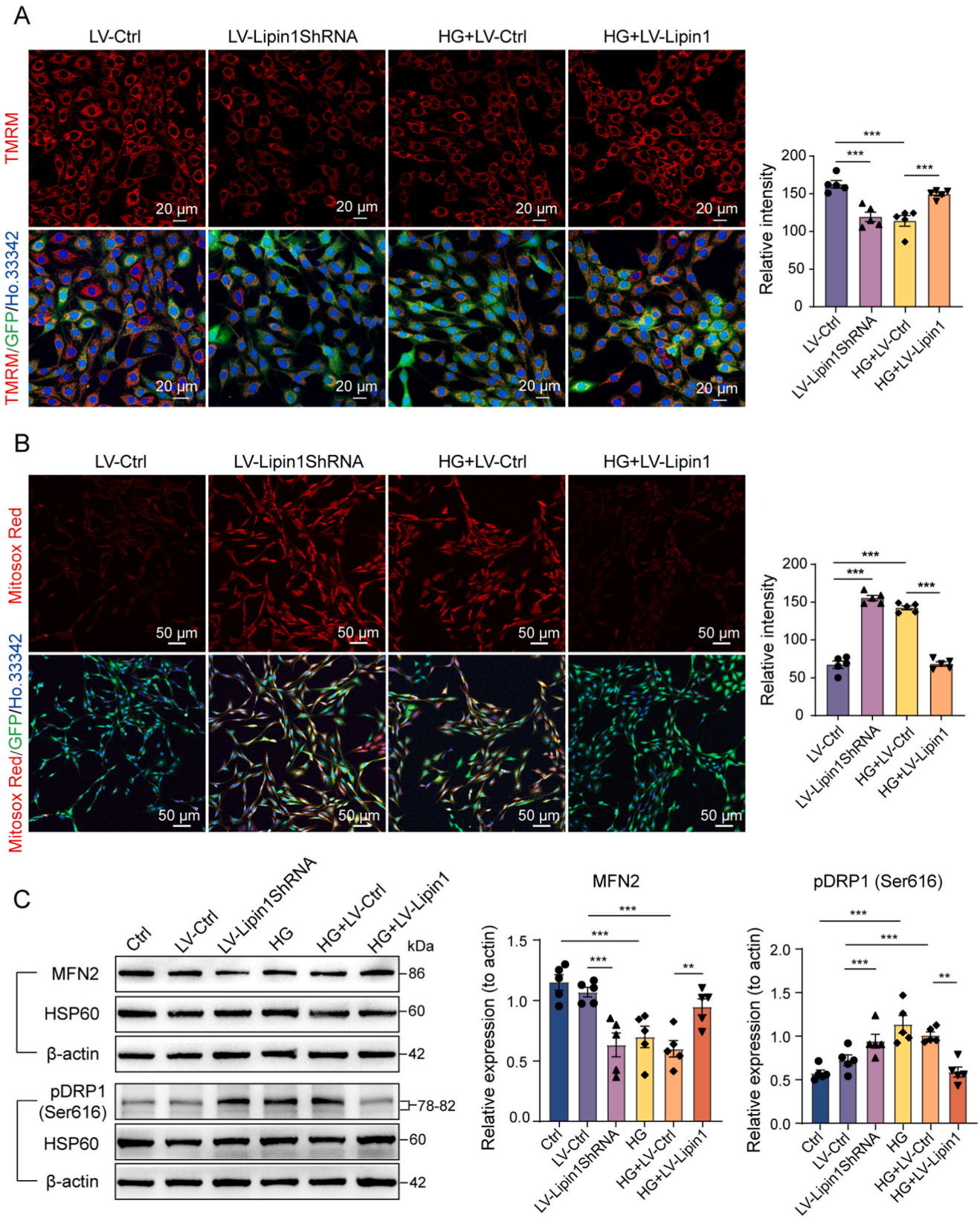

Fig. 8. Lipin1 effects upon mitochondrial function and dynamics in PC12 cells.
(A) Relative intensities of TMRM staining in PC12 cells within the LV-Ctrl, LV-Lipin1ShRNA, HG + LV-Ctrl and HG + LV-Lipin1 groups (n = 5). Scale bar is 20 μm. **(B)** Relative intensities of Mitosox Red staining in PC12 cells within the LV-Ctrl, LV-Lipin1ShRNA, HG + LV-Ctrl and HG-LV-Lipin1 groups (n = 5). Scale bar is 50 μm. **(C)** Relative expression levels of MFN2 and pDRP1 (Ser616) within the control, LV-Ctrl, LV-Lipin1ShRNA, HG, HG + LV-Ctrl and HG + LV-Lipin1 groups as determined using WB and analysis of WB with β-actin used as an internal reference (n = 5). All data represent means ± SEMs. $^{*}P < 0.05$, $^{**}P < 0.01$ and $^{***}P < 0.001$, by one-way ANOVA with LSD or Tamhane tests used for post-hoc comparisons. (For interpretation of the references to color in this figure legend, the reader is referred to the Web version of this article.)

function. Some of these studies concern Lipin1-associated myopathy, and it is reported that the loss of Lipin1 in muscle tissue is associated with a blockade in autophagic flux and accumulation of aberrant mitochondria [51–53]. Conclusion of what these studies agree with us is that Lipin1 plays a protective role in mitochondrial function, while the pattern of manifestation seems different. Among the studies, findings of Sellers RS et al. [52] and Schweitzer GG et al. [51] exhibit the increase of total mitochondrial content when Lipin1 is knocked out in muscle tissue, but the volume of individual mitochondrion has not been measured. Zhang P et al. demonstrate that the *fld/fld* soleus muscle exhibits large, misshapen mitochondria, and the effect is due to the blockage of autophagy by diminishing DAG-PKD-Vps34 pathway activation [53]. In addition, Huang H et al. propose that PA production on mitochondrial surface recruits Lipin1b and induces a conformational change that exposes the catalytic domain, leading to mitochondrial fission through production of DAG with the use of HeLa cells and NIH3T3 cells [54]. Results above indicate that there may be different mechanisms of Lipin1 on mitochondrial morphology and dynamics in different tissues, cell types and disease models and the differences are worthy of further investigations in future studies.

On the other hand, it is notable that Lipin1 have a dual role in regulation of gene expression besides the PAP activity for lipid biosynthesis [55]. Lipin1 can localize to nucleus and acts as a transcriptional coactivitor associated with fatty acid oxidation (FAO). Lipin1 is induced in liver by fasting and interacts directly with PPARγ coactivator-1α (PGC-1α) and peroxisome proliferators-activated receptor α (PPARα) to form a complex that stimulates FAO-related gene transcription [56]. In addition, Lipin1 in adipocytes induces expression of adipogenic key transcription factors PPARγ and C/EBPα, as well as lipogenic genes including fatty acid synthase, acetyl-CoA carboxylase, and diacylglycerol acyltransferase (DGAT) [55]. At present, the relationship between Lipin1 PAP and transcriptional activities is still controversial, and Lipin1 co-activator/co-repressor activity may function independently of PAP activity or may be supported by PAP activity [57]. In hepatic and adipose tissue, it is demonstrated that Lipin1 could present bi-functional cooperativity in response to some environmental stimulus like fasting, and then regulate the downstream lipid metabolic processes synergistically [58]. Recently, Lin S et al. reported that in renal proximal tubular epithelial cells (PTEC) of diabetic kidney disease (DKD), Lipin1 deficiency promoted fat synthesis and resulted in mitochondrial dysfunction by downregulating FAO via inhibiting PGC-1α/PPARα mediated Cpt1α/HNF4α signaling and upregulating SREBPs [59]. The study provides a hint that effects of Lipin1 on mitochondrial function in DE may be also led by the coordination of both PAP activity and transcriptional activity. Although we have demonstrated the function of Lipin1 PAP activity in this study, it remains unclear whether the transcriptional activity related to FAO or lipid metabolism is involved and further studies are required to illustrate it.

There are some limitations associated with this study. First, as we did not use AAVs that could be specifically transfected in neurons or a gene-edited animal that specifically knocked-down Lipin1 in neurons, a definitive demonstration that Lipin1 effects in neurons could not be completely established. Neuronal *in vitro* models we used partially remedy this limitation. Second, somewhat more valid and reliable results may have been obtained if we isolated mitochondria or mitochondrial membranes for the detection of phospholipids, as the biological characteristics of membranes on different sites or organelles can show variations. Finally, without employing site-directed mutations of the enzymatic or transcriptional co-activator functions, we could not exclude the transcriptional co-activator function of Lipin1 in DE besides its enzymatic activity.

In conclusion, the results presented in this study demonstrate that phosphatidate phosphatase Lipin1 involves in pathogenesis of diabetic encephalopathy via regulating synaptic mitochondrial dynamics. A Lipin1 deficiency that occurs under conditions of hyperglycemia disrupts the homeostasis of synaptic mitochondrial dynamics via reducing mitochondrial membrane phospholipids. Such effects eventually lead to a disorder in synaptic mitochondrial function, synaptic plasticity and finally, deficits in cognition. In contrast, the up-regulation of Lipin1 within hippocampal neurons in a diabetic encephalopathy model partially restores the cascade of dysfunction as described above. Accordingly, the findings of this study highlight the underlying therapeutic effect of Lipin1 and provide a possible target for the clinical treatment of DE.

Funding information

This work was supported by the National Natural Science Foundation of China (grant numbers 82070847, 82270869, 82170828, 81670753, and 81800722) and the Natural Science Foundation of Shandong Province (grant number ZR2021LSW016).

Authors' contributions

Conceptualization: XHZ, SYY, SHC; Data curation and formal analysis: XLH; Methodology: XLH, SH, XHZ, SYY, SHC; Investigation: XLH, SH, ZYZ, XCZ, MX, MYH; Visualization: XLH, NJL; Supervision: XHZ, SYY, SHC; Writing—original draft: XLH; Writing—review & editing: XLH, XHZ, SYY, SHC.

Data availability

Data are available from the corresponding authors on reasonable request.

Declaration of competing interest

The authors declare that they have no competing interests.

Acknowledgement

We specifically want to thank the members of Professor Shu-yan Yu's team, Ye Li, Cui-qin Fan, Tian Lan, Wen-jing Wang and Chang-min Wang (Department of Physiology, School of Basic Medical Sciences, Cheeloo College of Medicine, Shandong University) for their kindly help and guidance with the animal experiments.

Appendix A. Supplementary data

Supplementary data to this article can be found online at https://doi.org/10.1016/j.redox.2023.102996.

References

[1] R. Chen, J. Shi, Q. Yin, X. Li, Y. Sheng, J. Han, P. Zhuang, Y. Zhang, Morphological and pathological characteristics of brain in diabetic encephalopathy, J. Alzheimers Dis. 65 (1) (2018) 15–28.
[2] E. Reske-Nielsen, K. Lundbaek, Diabetic encephalopathy. Diffuse and focal lesions of the brain in long-term diabetes, Acta Neurol. Scand. Suppl. 39 (4) (1963) 273–290. SUPPL4.
[3] T. Xu, J. Liu, X.R. Li, Y. Yu, X. Luo, X. Zheng, Y. Cheng, P.Q. Yu, Y. Liu, The mTOR/NF-kappaB pathway mediates neuroinflammation and synaptic plasticity in diabetic encephalopathy, Mol. Neurobiol. 58 (8) (2021) 3848–3862.
[4] A. Artola, Diabetes-, stress- and ageing-related changes in synaptic plasticity in hippocampus and neocortex–the same metaplastic process? Eur. J. Pharmacol. 585 (1) (2008) 153–162.
[5] V. Todorova, A. Blokland, Mitochondria and synaptic plasticity in the mature and aging nervous system, Curr. Neuropharmacol. 15 (1) (2017) 166–173.
[6] J. Tang, A. Oliveros, M.H. Jang, Dysfunctional mitochondrial bioenergetics and synaptic degeneration in alzheimer disease, Int. Neurourol. J. 23 (Suppl 1) (2019) S5–S10.
[7] D.C. Altieri, Mitochondrial dynamics and metastasis, Cell. Mol. Life Sci. 76 (5) (2019) 827–835.
[8] J.M. Suarez-Rivero, M. Villanueva-Paz, P. de la Cruz-Ojeda, M. de la Mata, D. Cotan, M. Oropesa-Avila, I. de Lavera, M. Alvarez-Cordoba, R. Luzon-Hidalgo, J. A. Sanchez-Alcazar, Mitochondrial dynamics in mitochondrial diseases, Diseases 5 (1) (2016).

[9] M. Giacomello, A. Pyakurel, C. Glytsou, L. Scorrano, The cell biology of mitochondrial membrane dynamics, Nat. Rev. Mol. Cell Biol. 21 (4) (2020) 204–224.

[10] C. Osman, D.R. Voelker, T. Langer, Making heads or tails of phospholipids in mitochondria, J. Cell Biol. 192 (1) (2011) 7–16.

[11] M. Xie, M. Wang, W. Liu, M. Xu, P. Shang, D. Jiang, L. Ju, F. Wu, A. Sun, S. Yu, X. Zhuang, S. Chen, Lipin1 is involved in the pathogenesis of diabetic encephalopathy through the PKD/Limk/Cofilin signaling pathway, Oxid. Med. Cell. Longev. 2020 (2020), 1723423.

[12] M. Peterfy, J. Phan, P. Xu, K. Reue, Lipodystrophy in the fld mouse results from mutation of a new gene encoding a nuclear protein, lipin, Nat. Genet. 27 (1) (2001) 121–124.

[13] G. Yigitturk, A.C. Acara, O. Erbas, F. Oltulu, N.U.K. Yavasoglu, A. Uysal, A. Yavasoglu, The antioxidant role of agomelatine and gallic acid on oxidative stress in STZ induced type I diabetic rat testes, Biomed. Pharmacother. 87 (2017) 240–246.

[14] T. Xu, Z. Yu, Y. Liu, M. Lu, M. Gong, Q. Li, Y. Xia, B. Xu, Hypoglycemic effect of electroacupuncture at ST25 through neural regulation of the pancreatic intrinsic nervous system, Mol. Neurobiol. 59 (1) (2022) 703–716.

[15] X. Zhang, S. Huang, Z. Zhuang, X. Han, M. Xie, S. Yu, M. Hua, Z. Liang, C. Meng, L. Yin, X. Zhuang, S. Chen, Lipin2 ameliorates diabetic encephalopathy via suppressing JNK/ERK-mediated NLRP3 inflammasome overactivation, Int. Immunopharm. 118 (2023), 109930.

[16] Q. Zhang, Y. Tamura, M. Roy, Y. Adachi, M. Iijima, H. Sesaki, Biosynthesis and roles of phospholipids in mitochondrial fusion, division and mitophagy, Cell. Mol. Life Sci. 71 (19) (2014) 3767–3778.

[17] A. Marseglia, L. Fratiglioni, G. Kalpouzos, R. Wang, L. Backman, W. Xu, Prediabetes and diabetes accelerate cognitive decline and predict microvascular lesions: a population-based cohort study, Alzheimers Dement 15 (1) (2019) 25–33.

[18] Y. Liu, M. Li, Z. Zhang, Y. Ye, J. Zhou, Role of microglia-neuron interactions in diabetic encephalopathy, Ageing Res. Rev. 42 (2018) 28–39.

[19] Y. Xiong, T. Tian, Y. Fan, S. Yang, X. Xiong, Q. Zhang, W. Zhu, Diffusion tensor imaging reveals altered topological efficiency of structural networks in type-2 diabetes patients with and without mild cognitive impairment, J. Magn. Reson. Imag. 55 (3) (2022) 917–927.

[20] X.X. Fang, F.F. Xu, Z. Liu, B.B. Cao, Y.H. Qiu, Y.P. Peng, Interleukin 17A deficiency alleviates neuroinflammation and cognitive impairment in an experimental model of diabetic encephalopathy, Neural Regen Res. 17 (12) (2022) 2771–2777.

[21] Y. Tu, Q. Chen, W. Guo, P. Xiang, H. Huang, H. Fei, L. Chen, Y. Yang, Z. Peng, C. Gu, X. Tan, X. Liu, Y. Lu, R. Chen, H. Wang, Y. Luo, J. Yang, MiR-702-5p ameliorates diabetic encephalopathy in db/db mice by regulating 12/15-LOX, Exp. Neurol. 358 (2022), 114212.

[22] G. Neves, S.F. Cooke, T.V. Bliss, Synaptic plasticity, memory and the hippocampus: a neural network approach to causality, Nat. Rev. Neurosci. 9 (1) (2008) 65–75.

[23] J.J. Shi, H.F. Liu, T. Hu, X. Gao, Y.B. Zhang, W.R. Li, Q. Wang, S.J. Zhang, D. Tang, Y.B. Chen, Danggui-Shaoyao-San improves cognitive impairment through inhibiting O-GlcNAc-modification of estrogen alpha receptor in female db/db mice, J. Ethnopharmacol. 281 (2021), 114562.

[24] S.J. Liu, C. Yang, Y. Zhang, R.Y. Su, J.L. Chen, M.M. Jiao, H.F. Chen, N. Zheng, S. Luo, Y.B. Chen, S.J. Quan, Q. Wang, Neuroprotective effect of beta-asarone against Alzheimer's disease: regulation of synaptic plasticity by increased expression of SYP and GluR1, Drug Des. Dev. Ther. 10 (2016) 1461–1469.

[25] F.J. Bustos, E. Ampuero, N. Jury, R. Aguilar, F. Falahi, J. Toledo, J. Ahumada, J. Lata, P. Cubillos, B. Henriquez, M.V. Guerra, J. Stehberg, R.L. Neve, N. C. Inestrosa, U. Wyneken, M. Fuenzalida, S. Hartel, M. Sena-Esteves, L. Varela-Nallar, M.G. Rots, M. Montecino, B. van Zundert, Epigenetic editing of the Dlg4/PSD95 gene improves cognition in aged and Alzheimer's disease mice, Brain 140 (12) (2017) 3252–3268.

[26] P. Mitchell, Coupling of phosphorylation to electron and hydrogen transfer by a chemi-osmotic type of mechanism, Nature 191 (1961) 144–148.

[27] L. Doblado, C. Lueck, C. Rey, A.K. Samhan-Arias, I. Prieto, A. Stacchiotti, M. Monsalve, Mitophagy in human diseases, Int. J. Mol. Sci. 22 (8) (2021).

[28] W. Neupert, J.M. Herrmann, Translocation of proteins into mitochondria, Annu. Rev. Biochem. 76 (2007) 723–749.

[29] L. Vaillant-Beuchot, A. Mary, R. Pardossi-Piquard, A. Bourgeois, I. Lauritzen, F. Eysert, P.F. Kinoshita, J. Cazareth, C. Badot, K. Fragaki, R. Bussiere, C. Martin, R. Mary, C. Bauer, S. Pagnotta, V. Paquis-Flucklinger, V. Buee-Scherrer, L. Buee, S. Lacas-Gervais, F. Checler, M. Chami, Accumulation of amyloid precursor protein C-terminal fragments triggers mitochondrial structure, function, and mitophagy defects in Alzheimer's disease models and human brains, Acta Neuropathol. 141 (1) (2021) 39–65.

[30] R.Z. Zhao, S. Jiang, L. Zhang, Z.B. Yu, Mitochondrial electron transport chain, ROS generation and uncoupling (Review), Int. J. Mol. Med. 44 (1) (2019) 3–15.

[31] S. Orrenius, V. Gogvadze, B. Zhivotovsky, Mitochondrial oxidative stress: implications for cell death, Annu. Rev. Pharmacol. Toxicol. 47 (2007) 143–183.

[32] O.L. Erukainure, O.M. Ijomone, O. Sanni, M. Aschner, M.S. Islam, Type 2 diabetes induced oxidative brain injury involves altered cerebellar neuronal integrity and elemental distribution, and exacerbated Nrf2 expression: therapeutic potential of raffia palm (Raphia hookeri) wine, Metab. Brain Dis. 34 (5) (2019) 1385–1399.

[33] X. Pang, E.A. Makinde, F.N. Eze, O.J. Olatunji, Securidaca inappendiculata polyphenol rich extract counteracts cognitive deficits, neuropathy, neuroinflammation and oxidative stress in diabetic encephalopathic rats via p38 MAPK/Nrf2/HO-1 pathways, Front. Pharmacol. 12 (2021), 737764.

[34] W. Wang, F. Zhao, X. Ma, G. Perry, X. Zhu, Mitochondria dysfunction in the pathogenesis of Alzheimer's disease: recent advances, Mol. Neurodegener. 15 (1) (2020) 30.

[35] P.V.S. Vasileiou, K. Evangelou, K. Vlasis, G. Fildisis, M.I. Panayiotidis, E. Chronopoulos, P.G. Passias, M. Kouloukoussa, V.G. Gorgoulis, S. Havaki, Mitochondrial homeostasis and cellular senescence, Cells 8 (7) (2019).

[36] X. Wang, B. Su, H.G. Lee, X. Li, G. Perry, M.A. Smith, X. Zhu, Impaired balance of mitochondrial fission and fusion in Alzheimer's disease, J. Neurosci. 29 (28) (2009) 9090–9103.

[37] P. Mishra, D.C. Chan, Mitochondrial dynamics and inheritance during cell division, development and disease, Nat. Rev. Mol. Cell Biol. 15 (10) (2014) 634–646.

[38] A.B. Knott, G. Perkins, R. Schwarzenbacher, E. Bossy-Wetzel, Mitochondrial fragmentation in neurodegeneration, Nat. Rev. Neurosci. 9 (7) (2008) 505–518.

[39] M. Manczak, M.J. Calkins, P.H. Reddy, Impaired mitochondrial dynamics and abnormal interaction of amyloid beta with mitochondrial protein Drp1 in neurons from patients with Alzheimer's disease: implications for neuronal damage, Hum. Mol. Genet. 20 (13) (2011) 2495–2509.

[40] Y. Zhou, S. Lian, J. Zhang, D. Lin, C. Huang, L. Liu, Z. Chen, Mitochondrial perturbation contributing to cognitive decline in streptozotocin-induced type 1 diabetic rats, Cell. Physiol. Biochem. 46 (4) (2018) 1668–1682.

[41] L. Zhou, W. Wang, C. Hoppel, J. Liu, X. Zhu, Parkinson's disease-associated pathogenic VPS35 mutation causes complex I deficits, Biochim. Biophys. Acta, Mol. Basis Dis. 1863 (11) (2017) 2791–2795.

[42] W. Liu, R. Acin-Perez, K.D. Geghman, G. Manfredi, B. Lu, C. Li, Pink1 regulates the oxidative phosphorylation machinery via mitochondrial fission, Proc. Natl. Acad. Sci. U.S.A. 108 (31) (2011) 12920–12924.

[43] S.E. Horvath, G. Daum, Lipids of mitochondria, Prog. Lipid Res. 52 (4) (2013) 590–614.

[44] S. Eid, K.M. Sas, S.F. Abcouwer, E.L. Feldman, T.W. Gardner, S. Pennathur, P. E. Fort, New insights into the mechanisms of diabetic complications: role of lipids and lipid metabolism, Diabetologia 62 (9) (2019) 1539–1549.

[45] P. Shang, F. Zheng, F. Han, Y. Song, Z. Pan, S. Yu, X. Zhuang, S. Chen, Lipin1 mediates cognitive impairment in fld mice via PKD-ERK pathway, Biochem. Biophys. Res. Commun. 525 (2) (2020) 286–291.

[46] J.E. Vance, Phospholipid synthesis and transport in mammalian cells, Traffic 16 (1) (2015) 1–18.

[47] E.P. Kennedy, S.B. Weiss, The function of cytidine coenzymes in the biosynthesis of phospholipides, J. Biol. Chem. 222 (1) (1956) 193–214.

[48] G. van Meer, D.R. Voelker, G.W. Feigenson, Membrane lipids: where they are and how they behave, Nat. Rev. Mol. Cell Biol. 9 (2) (2008) 112–124.

[49] E.Y. Chan, G.A. McQuibban, Phosphatidylserine decarboxylase 1 (Psd1) promotes mitochondrial fusion by regulating the biophysical properties of the mitochondrial membrane and alternative topogenesis of mitochondrial genome maintenance protein 1 (Mgm1), J. Biol. Chem. 287 (48) (2012) 40131–40139.

[50] Y. Kageyama, Z. Zhang, H. Sesaki, Mitochondrial division: molecular machinery and physiological functions, Curr. Opin. Cell Biol. 23 (4) (2011) 427–434.

[51] G.G. Schweitzer, S.L. Collier, Z. Chen, K.S. McCommis, S.K. Pittman, J. Yoshino, S. J. Matkovich, F.F. Hsu, R. Chrast, J.M. Eaton, T.E. Harris, C.C. Weihl, B.N. Finck, Loss of lipin 1-mediated phosphatidic acid phosphohydrolase activity in muscle leads to skeletal myopathy in mice, Faseb. J. 33 (1) (2019) 652–667.

[52] R.S. Sellers, S.R. Mahmood, G.S. Perumal, F.P. Macaluso, I.J. Kurland, Phenotypic modulation of skeletal muscle fibers in LPIN1-deficient lipodystrophic (fld) mice, Veterinary Pathol. 56 (2) (2019) 322–331.

[53] P. Zhang, M.A. Verity, K. Reue, Lipin-1 regulates autophagy clearance and intersects with statin drug effects in skeletal muscle, Cell Metabol. 20 (2) (2014) 267–279.

[54] H. Huang, Q. Gao, X. Peng, S.Y. Choi, K. Sarma, H. Ren, A.J. Morris, M.A. Frohman, piRNA-associated germline nuage formation and spermatogenesis require MitoPLD profusogenic mitochondrial-surface lipid signaling, Dev. Cell 20 (3) (2011) 376–387.

[55] K. Reue, P. Zhang, The lipin protein family: dual roles in lipid biosynthesis and gene expression, FEBS Lett. 582 (1) (2008) 90–96.

[56] B.N. Finck, M.C. Gropler, Z. Chen, T.C. Leone, M.A. Croce, T.E. Harris, J. C. Lawrence Jr., D.P. Kelly, Lipin 1 is an inducible amplifier of the hepatic PGC-1alpha/PPARalpha regulatory pathway, Cell Metabol. 4 (3) (2006) 199–210.

[57] L.S. Csaki, J.R. Dwyer, L.G. Fong, P. Tontonoz, S.G. Young, K. Reue, Lipins, lipinopathies, and the modulation of cellular lipid storage and signaling, Prog. Lipid Res. 52 (3) (2013) 305–316.

[58] T.E. Harris, B.N. Finck, Dual function lipin proteins and glycerolipid metabolism, Trends Endocrinol. Metabol.: TEM (Trends Endocrinol. Metab.) 22 (6) (2011) 226–233.

[59] S. Lin, L. Wang, Y. Jia, Y. Sun, P. Qiao, Y. Quan, J. Liu, H. Hu, B. Yang, H. Zhou, Lipin-1 deficiency deteriorates defect of fatty acid β-oxidation and lipid-related kidney damage in diabetic kidney disease. Translational Research : the Journal of Laboratory and Clinical Medicine, 2023.